8. Lin KJ, Hsu WC, Hsiao IT, Wey SP, Jin LW, Skovronsky D, Wai YY, Chang HP, Lo CW, Yao CH, Yen TC, Kung MP: **Whole-body biodistribution and brain PET imaging with [^{18}F]AV-45, a novel amyloid imaging agent–a pilot study.** *Nucl Med Biol* 2010, **37**:497–508.
9. Wong DF, Rosenberg PB, Zhou Y, Kumar A, Raymont V, Ravert HT, Dannals RF, Nandi A, Brasic JR, Ye W, Hilton J, Lyketsos C, Kung HF, Joshi AD, Skovronsky DM, Pontecorvo MJ: **In vivo imaging of amyloid deposition in Alzheimer disease using the radioligand ^{18}F-AV-45 (florbetapir [corrected] F 18).** *J Nucl Med* 2010, **51**:913–920.
10. Koole M, Lewis DM, Buckley C, Nelissen N, Vandenbulcke M, Brooks DJ, Vandenberghe R, Van Laere K: **Whole-body biodistribution and radiation dosimetry of ^{18}F-GE067: a radioligand for in vivo brain amyloid imaging.** *J Nucl Med* 2009, **50**:818–822.
11. O'Keefe GJ, Saunder TH, Ng S, Ackerman U, Tochon-Danguy HJ, Chan JG, Gong S, Dyrks T, Lindemann S, Holl G, Dinkelborg L, Villemagne V, Rowe CC: **Radiation dosimetry of beta-amyloid tracers ^{11}C-PiB and ^{18}F-BAY94-9172.** *J Nucl Med* 2009, **50**:309–315.
12. Furumoto S, Okamura N, Furukawa K, Tashiro M, Ishikawa Y, Sugi K, Tomita N, Waragai M, Harada R, Tago T, Iwata R, Yanai K, Arai H, Kudo Y: **A ^{18}F-labeled BF-227 derivative as a potential radioligand for imaging dense amyloid plaques by positron emission tomography.** *Mol Img Biol.* in press.
13. Fujiwara T, Watanuki S, Yamamoto S, Miyake M, Seo S, Itoh M, Ishii K, Orihara H, Fukuda H, Satoh T, Kitamura K, Tanaka K, Takahashi S: **Performance evaluation of a large axial field-of-view PET scanner: SET-2400W.** *Ann Nucl Med* 1997, **11**:307–313.
14. Watanuki S, Tashiro M, Miyake M, Ishikawa Y, Itoh M, Yanai K, Sakemi Y, Fukuda H, Ishii K: **Long-term performance evaluation of positron emission tomography: analysis and proposal of a maintenance protocol for long-term utilization.** *Ann Nucl Med* 2010, **24**:461–468.
15. Loevinger R, Budinger T, Watson E: *MIRD Primer for Absorbed Dose Calculations. Revised edn.* New York: The Society of Nuclear Medicine; 1991.
16. Cristy M, Eckerman KF: *Specific Absorbed Fractions of Energy at Various Ages from Internal Photon ources.* Oak Ridge: ORNL/TM; 1987:8381.
17. Stabin MG, Sparks RB, Crowe E: **OLINDA/EXM: the second-generation personal computer software for internal dose assessment in nuclear medicine.** *J Nucl Med* 2005, **46**:1023–1027.
18. Kirschner AS, Ice RD, Beierwaltes WH: **Radiation dosimetry of ^{131}I-19-iodocholesterol: the pitfalls of using tissue concentration data -reply.** *J Nucl Med* 1975, **16**:248–249.
19. Lartizien C, Comtat C, Kinahan PE, Ferreira N, Bendriem B, Trebossen R: **Optimization of injected dose based on noise equivalent count rates for 2- and 3-dimensional whole-body PET.** *J Nucl Med* 2002, **43**:1268–1278.
20. ICRP: *Radiological Protection in Biomedical Research.* Oxford: Pergamon; 1992.
21. Kimura Y, Simeon FG, Hatazawa J, Mozley PD, Pike VW, Innis RB, Fujita M: **Biodistribution and radiation dosimetry of a positron emission tomographic ligand, ^{18}F-SP203, to image metabotropic glutamate subtype 5 receptors in humans.** *Eur J Nucl Med Mol Imaging* 2010, **37**:1943–1949.
22. Directorate-General Environment NSaCP: **Guidance on medical exposures in medical and biomedical research.** In *Radiation Protection.* Brussels: European Commission; 1998:1–14.

doi:10.1186/2191-219X-3-32
Cite this article as: Shidahara *et al.*: Evaluation of the biodistribution and radiation dosimetry of the ^{18}F-labelled amyloid imaging probe [^{18}F] FACT in humans. *EJNMMI Research* 2013 **3**:32.

MOLECULAR IMAGING AND BIOLOGY

Mol Imaging Biol (2013)
DOI: 10.1007/s11307-012-0608-5

World Molecular Imaging Society

RESEARCH ARTICLE

A ^{18}F-Labeled BF-227 Derivative as a Potential Radioligand for Imaging Dense Amyloid Plaques by Positron Emission Tomography

Shozo Furumoto,[1,2] Nobuyuki Okamura,[1] Katsutoshi Furukawa,[3] Manabu Tashiro,[4] Yoichi Ishikawa,[2] Kentaro Sugi,[1] Naoki Tomita,[3] Masaaki Waragai,[3] Ryuichi Harada,[1] Tetsuro Tago,[2] Ren Iwata,[2] Kazuhiko Yanai,[1] Hiroyuki Arai,[3] Yukitsuka Kudo[5]

[1]*Department of Pharmacology, Tohoku University School of Medicine, 2-1 Seiryo-machi, Aoba-ku, Sendai 980-8575, Japan*
[2]*Division of Radiopharmaceutical Chemistry, Cyclotron and Radioisotope Center, Tohoku University, Sendai, Japan*
[3]*Department of Geriatrics and Gerontology, Division of Brain Sciences, Institute of Development, Aging and Cancer, Tohoku University, Sendai, Japan*
[4]*Division of Cyclotron Nuclear Medicine, Cyclotron and Radioisotope Center, Tohoku University, Sendai, Japan*
[5]*Clinical Research, Innovation and Education Center, Tohoku University Hospital, Sendai, Japan*

Abstract

Purpose: The aims of this study were to evaluate the binding and pharmacokinetics of novel ^{18}F-labeled ethenyl-benzoxazole derivatives (i.e., [^{18}F] fluorinated amyloid imaging compound of Tohoku university ([^{18}F]FACT)) as amyloid positron emission tomography (PET) tracers and to assess [^{18}F]FACT efficacy in imaging of Alzheimer's disease (AD).

Procedures: Binding assay was conducted using synthetic amyloid-β (Aβ) fibrils, fluorescence microscopy, and autoradiogram in three postmortem AD brains. Pharmacokinetics of [^{18}F]FACT was assessed using 12 Crj:CD-1 (ICR) mice. *In vivo* binding ability with brain amyloid was investigated using amyloid precursor protein (APP) transgenic mouse. Clinical PET scanning using [^{18}F]FACT was performed in ten healthy controls and ten mild cognitive impairment and ten AD patients.

Results: [^{18}F]FACT showed high binding affinity for synthetic Aβ fibrils, preferential binding to dense cored plaques in brain sections, and excellent brain uptake and rapid clearance in mice. Injection in APP mice resulted in specific *in vivo* labeling of amyloid deposits in the brain. PET scans of AD patients showed significantly higher [^{18}F]FACT uptake in the neocortex compared to controls ($P<0.05$, Kruskal–Wallis test).

Conclusion: [^{18}F]FACT is a promising agent for imaging dense Aβ plaques in AD.

Key words: Alzheimer's disease, Amyloid, Early diagnosis, Positron emission tomography

Introduction

Alzheimer's disease (AD) is an age-dependent and irreversible neurodegenerative disorder leading to deterioration of memory and cognitive function. Although the exact mechanisms underlying pathogenesis of AD are not fully understood, formation of brain amyloid plaques through aggregation and deposition of amyloid-β protein (Aβ) is considered to be the initial pathogenic event that may precede the appearance of clinical AD symptoms by decades. Recently, new criteria for diagnosing AD were proposed by the National Institute on Aging—Alzheimer's Association workgroups [1]. The new diagnostic criteria include the use of biomarkers for amyloid deposition to aid

Correspondence to: Nobuyuki Okamura; *e-mail:* nookamura@med.tohoku.ac.jp

Published online: 30 January 2013

in diagnosis of AD. Thus, *in vivo* detection of amyloid depositions with positron emission tomography (PET) has received much attention as a potential technology for early or presymptomatic diagnosis of AD. For this purpose, a number of radiotracers for Aβ aggregates have been synthesized and evaluated as candidates for PET amyloid imaging agents, and some of these are undergoing clinical investigation [2–4].

Among them, *N*-methyl-[^{11}C]-2-(4′-methylaminophenyl)-6-hydroxybenzothiazole ([^{11}C]Pittsburgh compound B, [^{11}C]PiB) is currently the most widely used in clinical research [5]. Labeling of PET tracers with ^{18}F ($T_{1/2}$= 109.8 min) allows time for their delivery to numerous PET centers and contributes to spreading their use. Several ^{18}F-labeled amyloid PET tracers, including [^{18}F]flutemetamol, [^{18}F]florbetaben, [^{18}F]florbetapir, and [^{18}F]AZD4694, have been developed, and to date, [^{18}F]florbetapir has become commercially available [6–9]. An increasing number of PET studies in humans have clearly demonstrated that amyloid PET is a potentially useful technique to visualize and quantify the distribution of Aβ plaques of AD patients [5]. In addition, a proportion of elderly normal subjects present with [^{11}C]PiB retention in the neocortex [10–12], suggesting that amyloid PET is potentially useful for presymptomatic detection of Aβ pathology. Although neocortical PiB retention is considered as a high risk for future cognitive decline, not all PiB-positive normal individuals are destined to develop dementia. Some additional biomarkers are thus necessary for accurate prediction of future conversion to dementia. According to previous histopathological study, progression to dementia is associated with a shift from non-fibrillar to fibrillar amyloid deposits in the brain [13]. Thus, selective detection of dense fibrillar amyloid might be advantageous for predicting progression to dementia.

Previously, we had succeeded in developing a unique scaffold of a radioligand, [^{11}C]2-(2-[2-dimethylaminothiazol-5-yl]ethenyl)-6-(2-[fluoro]ethoxy)benzoxazole ([^{11}C]BF-227), as an amyloid imaging probe [3, 14]. Our previous study demonstrated that Aβ deposits in AD patients can be clearly detected by [^{11}C]BF-227 PET [15]. Neocortical [^{11}C]BF-227 retention was further observed in subjects with mild cognitive impairment (MCI) [16]. Using [^{11}C]BF-227 PET, we achieved a sensitivity of 100 % and a specificity of 71.4 % in distinguishing MCI converters to AD from MCI non-converters [17], suggesting the usefulness of this radiotracer for accurate prediction of future progression to dementia. To further take advantage of this imaging potential, especially in a large clinical study, we anticipated that a ^{18}F-labeled derivative of BF-227 would be valuable due to the longer half-life of ^{18}F compared with ^{11}C.

In this study, we performed a biological evaluation of a series of ^{18}F-labeled 2-ethenyl-benzoxazole derivatives (Fig. 1) to select a candidate for clinical application. The one selected, [^{18}F]Fluorinated Amyloid Imaging Compound of Tohoku University ([^{18}F]FACT), was further evaluated for its binding characteristics with Aβ fibrils and plaques and then for its clinical utility as a probe for imaging amyloid in AD.

Methods

Radiosynthesis of ^{18}F-Labeled 2-Ethenyl-Benzoxazole Derivatives

The chemical structures of the 2-ethenyl-benzoxazole derivatives are summarized in Fig. 1. The compounds and their precursors for ^{18}F-labeling were synthesized according to the method described previously [18]. ^{18}F-labeled compounds were prepared according to the following method. The aqueous $^{18}F^-$ contained in K_2CO_3 solution (1.27 to 3.28 GBq) and Kryptofix 2.2.2 were put into a brown vial, and then the water was azeotropically removed with acetonitrile by heating at 110 °C and He-gas flow. After drying, the activated [^{18}F]KF/Kryptofix 2.2.2. was reacted with a tosylate precursor in dimethyl sulfoxide (DMSO) at 110 °C for 10 min, followed by addition of water to quench. The product was extracted by solid-phase extraction with Sep-Pak ^{t}C18 cartridge (Waters) and then eluted with ethanol. The ^{18}F-labeled compound was separated from the eluent by semi-preparative reversed-phase high-performance liquid chromatography (RP-HPLC), isolated from the collected fraction by solid-phase extraction with Sep-Pak ^{t}C18

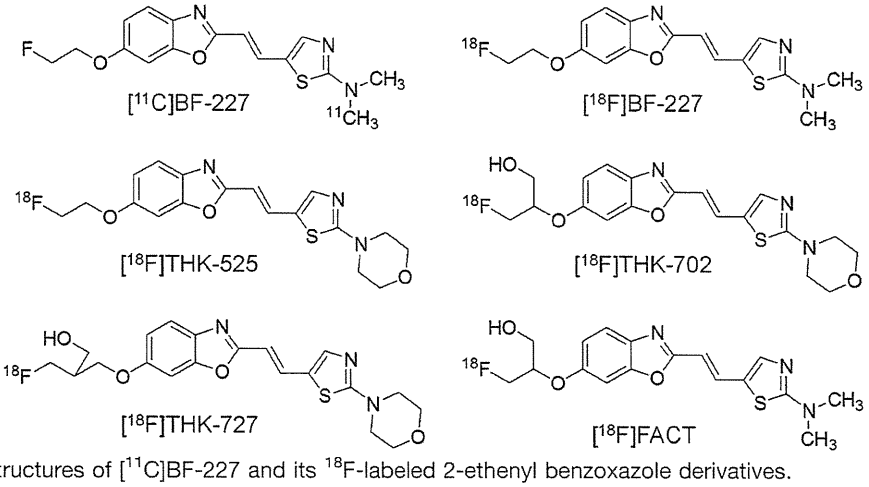

Fig. 1. Chemical structures of [^{11}C]BF-227 and its ^{18}F-labeled 2-ethenyl benzoxazole derivatives.

cartridge, and finally dissolved in DMSO or saline with polysorbate-80 (<0.1 %) for biological evaluation.

[^{11}C]BF-227 was synthesized from the precursor by *N*-methylation with [^{11}C]methyl triflate in DMSO and separated from the crude mixture by semi-preparative RP-HPLC, as described previously [15]. The purified [^{18}F]FACT and [^{11}C]BF-227 were solubilized in isotonic saline containing 1 % polysorbate-80 and 5 % ascorbic acid and then filter-sterilized with 0.22 μm Millipore filter for clinical use.

Fluorescent Staining

Postmortem brain tissue from a 69-year-old man with autopsy-confirmed AD was obtained from Fukushimura Hospital (Toyohashi, Japan). Experiments were performed under the regulations of the hospital ethics committee. Serial sections (6 μm) taken from paraffin-embedded blocks of the temporal cortex were prepared in xylene and ethanol. Before staining with test compounds, quenching of autofluorescence was performed. The quenched tissue section was immersed in 100 μM of test compounds containing 50 % ethanol for 10 min. The stained section was then dipped briefly into water before coverslipping with FluorSave Reagent (Calbiochem, La Jolla, CA, USA) and examination using an Eclipse E800 microscope (Nikon, Tokyo, Japan) equipped with a V-2A filter set (excitation 380 to 420 nm, dichroic mirror 430 nm, long pass filter 450 nm). An adjacent section was immunostained using 4G8 (Signet, Dedham, MA, USA), a monoclonal antibody against Aβ. After pretreatment with 90 % formic acid for 5 min, sections were immersed in blocking solution for 30 min and then incubated for 60 min at 37 °C with 4G8 at a dilution of 1:100. After incubation, sections were processed with biotinylated anti-mouse IgG (Wako) for 60 min, followed by Texas Red-conjugated streptavidin (Vector Laboratories, Burlingame, CA, USA).

In Vitro Autoradiography

A temporal brain section from a 76-year-old female AD patient was incubated with 1.85 MBq/ml of [^{18}F]FACT at room temperature for 20 min and then washed briefly with water and 70 % ethanol. After drying, the labeled section was exposed to a BAS-III imaging plate (Fuji Film, Tokyo, Japan) for 120 min. Autoradiograms were obtained using a BAS-5000 phosphor imaging instrument (Fuji Film, Tokyo, Japan). Neighboring sections were immunostained using 4G8 anti-Aβ monoclonal antibody. After incubation with 4G8, sections were processed by the avidin–biotin method using a Pathostain ABC-POD(M) Kit (Wako, Osaka, Japan) and diaminobenzidine tetrahydrochloride.

In Vitro Binding Study

Amyloid β_{1-40} (Peptide Institute, Inc., Japan) was dissolved in 50 mM potassium phosphate buffer (pH 7.4) to a final concentration of 20 μM. To prepare amyloid fibrils, the solution was incubated at 37 °C for 4 days at 85 rpm and then sonicated to obtain a uniform suspension. The fibril solution was diluted to 2 μM with phosphate-buffered saline (PBS) containing 0.1 % bovine serum albumin (BSA). For saturation binding assay, 100 μl of the fibril solution was mixed with [^{18}F]FACT solution (0.2 to 800 nM, PBS containing 0.1 % BSA and 2 % DMSO, 100 μl) in a 96-well plate. Non-specific binding was defined in the presence of 2 μM FACT in the final solution. The mixture was incubated for 40 min at room temperature and then was passed through the glass filter plate under vacuum with MultiScreen HTS Vacuum Manifold (Millipore Corp., USA), followed by washing with PBS containing 0.1 % BSA twice. Radioactivity of the filter was counted with an automatic gamma counter. The binding data were analyzed with curve-fitting software that calculates the K_d and B_{max} using non-linear regression (GraphPad Prism Version 5.0, GraphPad Software, San Diego, CA, USA).

Biodistribution Study in Normal Mice

The experimental protocols were reviewed by the Committee on the Ethics of Animal Experiments at Tohoku University School of Medicine and performed in accordance with the Guidelines for Animal Experiments issued by the Tohoku University School of Medicine. Male Crj:CD-1 (ICR) mice (6 weeks old, 25 to 30 g, n=12) were injected in a lateral tail vein with ^{18}F-labeled test compounds (370 to 740 kBq) contained in isotonic saline (0.2 ml). The mice were sacrificed by cervical dislocation following heart puncture to obtain blood samples at 2, 30, and 60 min postinjection (n=4 at each time point). Tissues of interest were excised and weighed, and the radioactivity was counted in an automatic gamma-counter. Radioactivity uptake data are expressed as percent of injected dose per gram of tissue (%ID/g).

Autoradiography of Aβ Deposits in Living Transgenic Mice

An amyloid precursor protein (APP) transgenic (Tg) mouse (female, 31 months old) and a wild-type littermate (female, 31 months old) were injected with [^{18}F]FACT (37 MBq) *via* tail vein. The mice were sacrificed by cervical dislocation at 2 h postinjection, and the brains were rapidly excised and frozen in liquid nitrogen. Frozen sections of 20 μm thick were prepared from the brains for *ex vivo* autoradiography. Autoradiograms were obtained in the same manner described above. The sections used for autoradiography were then subjected to fluorescent staining with thioflavin-S according to the previously described method [19].

Clinical PET Study Using [^{18}F]FACT

Ten patients with amnestic MCI, ten patients with AD, and ten normal age-matched controls participated in the clinical PET study using [^{18}F]FACT. Please refer to Table 1 for characteristics of participants. [^{11}C]BF-227 PET scan was additionally performed in two patients with AD (70-year-old woman (MMSE score 17) and 79-year-old man (MMSE score 20)) and 1 normal control subject (60-year-old man (MMSE score 30)). The average time interval between [^{18}F]FACT and [^{11}C]BF-227 PET scans was 12±6 months. Diagnosis of probable AD was based on criteria from the National Institute of Neurological and Communicative Disorders and Stroke and the Alzheimer's Disease Related Disorders Association [20]. The diagnosis of amnestic MCI was made according to published criteria described previously [21]. The control subjects were

Table 1. Subject and patient demographics in [^{18}F]FACT PET comparisons

	NC	MCI	AD
N	10	10	10
Gender (F/M)	4/6	7/3	7/3
Age (years)	69.8±8.8 (60–89)	74.2±8.8 (57–89)	74.5±4.6 (66–81)
MMSE score	29.9±0.3 (29–30)	26.4±1.1 (24–28)	19.8±3.0 (15–24)

recruited from volunteers who were taking no centrally acting medications, had no cognitive impairment, and had no cerebrovascular lesions, including asymptomatic cerebral infarction on T2-weighted studies, identified *via* MRI. All volunteers were screened using a questionnaire and medical history, and those with medical conditions potentially affecting the central nervous system were excluded. The Committee on Clinical Investigation at Tohoku University School of Medicine and the Advisory Committee on Radioactive Substances at Tohoku University approved the study protocol. After complete description of the study to the patients and subjects, written informed consent was obtained.

Image Acquisition Protocols

[^{18}F]FACT-PET and [^{11}C]BF-227-PET study was performed using a SET-2400W PET scanner (Shimadzu, Kyoto, Japan). After intravenous injection of 111–185 MBq of [^{18}F]FACT or 211–366 MBq of [^{11}C]BF-227, dynamic PET images were obtained for 60 min (23 sequential scans; 5 scans×30 s, 5 scans×60 s, 5 scans×150 s, and 8 scans×300 s) with the subject's eyes closed. SUV summation images at 0–10, 10–20, 20–30, 30–40, 40–50, and 50–60 min postinjection were created for the analysis of tracer uptake. T1-weighted MR images were obtained using a SIGNA 1.5 T machine (General Electric, Milwaukee, WI, USA).

Image Analysis

Firstly, standardized uptake value (SUV) images of [^{18}F]FACT and [^{11}C]BF-227 were obtained by normalizing tissue radioactivity concentration by injected dose and body weight. Subsequently, individual MR images were anatomically coregistered into individual PET images using Statistical Parametric Mapping software (SPM5: Welcome Department, UK). Regions of interest (ROIs) were placed on individual axial MR images in the cerebellar hemisphere, frontal cortex [Brodmann's areas (BA) 8, 9, 10, 44, 45, 46, and 47], lateral temporal cortex (BA 21, 22, 37, and 38), parietal cortex (BA 39 and 40), occipital cortex (BA 17), anterior cingulate cortex, posterior cingulate cortex, medial temporal cortex (BA 27, 28, 34, and 35), striatum, pons, and subcortical white matter, as described previously [15]. The ROI information was then copied onto dynamic PET SUV images, and regional SUVs were sampled using PMOD software (PMOD Technologies, Ltd., Zurich, Switzerland). The ratio of regional SUV to cerebellar SUV (SUVR) was calculated as an index of tracer retention. Averaged SUVR in the frontal, temporal, parietal, and posterior cingulate cortices was considered representative of tracer retention in the neocortex (neocortical SUVR). The inter-rater reliability for the ROI measurement was tested between two raters (N.O. and K.S.) in seven subjects and patients. The intra-class correlation coefficient was 0.95.

Statistical Analysis

For statistical comparison in the three groups, we applied the Kruskal–Wallis test followed by Dunn's multiple comparison test. Differences of time activity curves (TACs) in [^{18}F]FACT PET were also evaluated by repeated measures ANOVA followed by the Bonferroni–Dunn post hoc test. For statistical comparisons of PET measurements in control and AD groups, we used the Mann–Whitney *U* test. Effect size coefficients (Cohen's *d*) were also calculated for the evaluation of group differences in PET measurements. Statistical significance for each analysis was defined as $P<0.05$. Correlations between [^{18}F]FACT and [^{11}C]BF-227 SUVR in the frontal, temporal, parietal, and occipital cortices of three subjects (two AD and one normal control) were determined using Pearson's correlations. A linear model was applied to the data to obtain a correlation coefficient and *p* value. These analyses were performed using GraphPad Prism5 software (GraphPad, San Diego, CA, USA).

Results

Radiosynthesis

^{18}F-labeled 2-ethenyl-benzoxazole derivatives (Fig. 1) were obtained in yields of 32 % on average (21 to 44 %, decay-corrected) with radiochemical purity greater than 99 % after HPLC purification. The specific activities ranged 70 to 180 GBq/μmol, corrected at the end of synthesis.

In Vitro Binding to Aβ Plaques in AD Brain Sections

Binding ability of 2-ethenyl-benzoxazole derivatives to Aβ plaques was examined using AD brain sections from a 69-year-old man with autopsy-confirmed AD. As shown in Fig. 2a, c, dense cored plaques (arrowheads) were clearly stained with FACT. In particular, Aβ plaque cores were brightly stained with this compound. The fluorescent staining pattern of FACT correlated well with Aβ immunostaining (Fig. 2b) and thioflavin-S staining (Fig. 2d) in adjacent sections. Other compounds produced similar results in the histopathological staining of AD brain sections from a 69-year-old man with autopsy-confirmed AD.

In vitro autoradiography at tracer dose indicated [^{18}F]FACT binding to dense Aβ deposits (arrowheads) in AD temporal brain sections from a 76-year-old female AD patient (Fig. 2e–h). Tracer signals were additionally detected

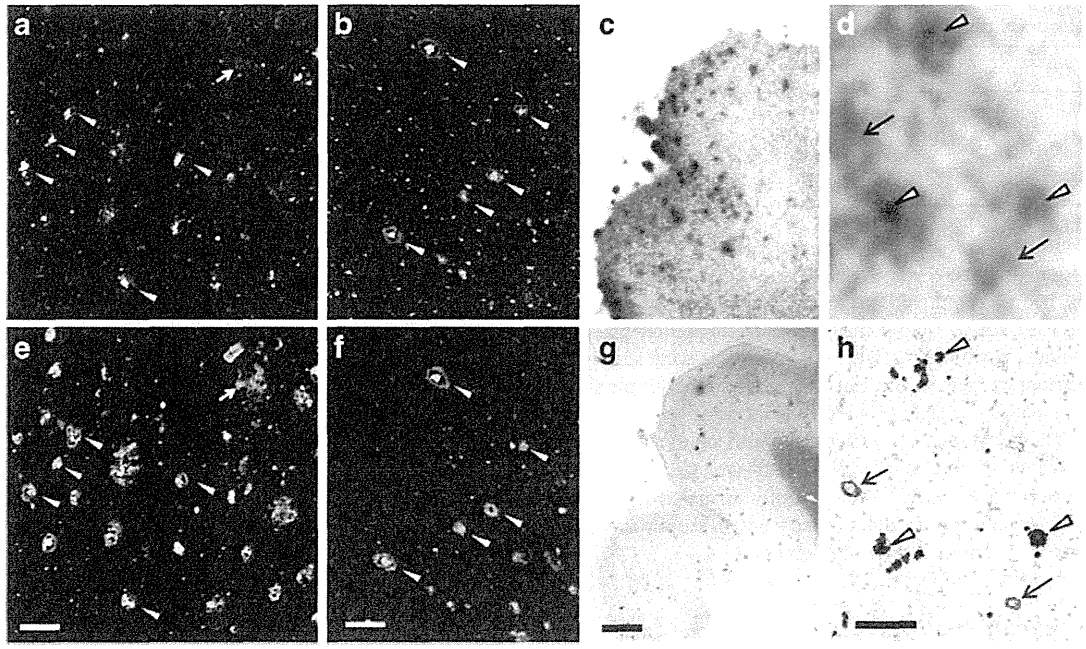

Fig. 2. **a–d** Fluorescence microscopy images of AD brain sections from a 69-year-old man with autopsy-confirmed AD stained with FACT (**a**, **c**), anti-Aβ (4 G8) antibody (**b**), and thioflavin-S (**d**). *Arrowheads* delineate dense cored plaques, respectively. **e–h** Autoradiogram of AD brain section from a 76-year-old female AD patient with [^{18}F]FACT (**e**, **g**) and images of the adjacent section immunostained with anti-Aβ (4 G8) antibody (**f**, **h**). *Arrows* and *arrowheads* delineate congophilic amyloid angiopathy and dense cored plaques, respectively. *Bars* 100 μm (**a–d**), 2 mm (**e–f**), 200 μm (**g–h**).

in congophilic amyloid angiopathy (arrows). These results indicated that FACT and its derivatives had an ability to detect pathological dense Aβ deposits in AD brain tissue.

Binding Affinity to Synthetic Aβ Fibrils

Binding properties of [^{18}F]FACT with Aβ fibrils were investigated by *in vitro* binding assay. Scatchard analysis of FACT binding to Aβ fibrils showed two classes of binding sites: a high-affinity site (K_d=9.4 nM; B_{max}= 0.16 pmol/nmol of Aβ) and a low-affinity site (K_d= 263 nM; B_{max}=1.52 pmol/nmol of Aβ).

Biodistribution Study in Normal Mice

Two important properties of an amyloid imaging probe are rapid brain uptake and rapid clearance from the normal brain without non-specific binding. These properties of the ^{18}F-labeled 2-ethenyl-benzoxazole derivatives were evaluated by biodistribution studies in 12 normal mice (n=4 at each time point). The radioactivity uptake in the blood, brain, liver, kidney, and bone is summarized in Table 2. Regarding brain uptake, all of the ^{18}F-labeled derivatives showed rapid and sufficient brain uptake (4 to 6 %ID/g at 2 min) and smooth washout after that. However, the brain uptake at 60 min varied from 0.28 to 1.68 %ID/g, suggesting a different clearance property in normal brain. Among the derivatives, [^{18}F]FACT indicated the highest ratio of brain uptakes at 2 min to that at 60 min (4.64/0.28=16.6). Additionally, mice injected with [^{18}F]FACT exhibited no increase of the radioactivity uptake in bone with time, unlike with [^{18}F]BF-227, suggesting that [^{18}F] FACT has good stability in regard to metabolic defluorination *in vivo*. Thus, we selected [^{18}F]FACT as the candidate for the clinical comparisons.

Autoradiography of Aβ Deposits in Living Transgenic Mouse

In vivo binding ability of [^{18}F]FACT with amyloid plaques was evaluated in the APP-Tg mouse. Autoradiographic images of the APP-Tg mouse brain post-intravenous injection of [^{18}F]FACT displayed high uptake of the labeling compound in the cortex and hippocampus (Fig. 3a). In contrast, no notable binding was observed in the brain of wild-type mouse (Fig. 3b). These [^{18}F]FACT binding results in APP-Tg mouse brain corresponded closely with those of *in vitro* thioflavin-S staining in the same brain sections (Fig. 3c, d). These results warranted further clinical investigation of [^{18}F]FACT PET in AD patients.

Clinical PET Study Using [^{18}F]FACT

Demographic data for the participants are summarized in Table 1. No statistical difference in age was observed among the three groups. MCI and AD patients had significantly lower mean MMSE scores than normal controls (P<0.05,

Table 2. Biodistribution of ^{18}F-labeled compounds in mice

Tracers	Time (min)	Radioactivity uptakes (%ID/g)				
		Blood	Brain	Liver	Kidney	Bone
[^{18}F]BF-227	2	2.93±0.08	6.05±0.45	7.97±1.59	9.63±0.89	1.59±0.27
	30	2.14±0.17	1.91±0.05	5.75±0.42	3.04±0.15	4.38±1.24
	60	2.09±0.15	1.67±0.14	5.48±0.23	2.42±0.20	7.04±0.75
[^{18}F]THK-525	2	2.82±0.38	4.73±1.32	5.93±1.40	7.72±2.44	1.77±0.87
	30	2.20±0.24	2.05±0.16	3.55±0.60	2.32±0.18	6.74±2.20
	60	1.91±0.29	1.68±0.15	2.47±0.23	1.48±0.14	9.65±0.89
[^{18}F]THK-702	2	3.34±0.13	4.15±0.28	7.53±0.50	13.6±0.88	1.95±0.34
	30	1.06±0.19	0.53±0.03	4.55±0.39	1.58±0.64	0.92±0.11
	60	0.67±0.08	0.35±0.04	3.65±0.72	0.65±0.09	1.16±0.70
[^{18}F]THK-727	2	2.94±0.33	4.06±0.26	9.89±4.16	11.4±1.35	2.08±0.39
	30	1.52±0.10	1.04±0.08	6.68±1.22	2.47±0.36	6.61±0.79
	60	0.66±0.10	0.69±0.02	4.04±1.87	0.98±0.14	9.33±1.34
[^{18}F]FACT	2	3.65±0.66	4.64±0.55	9.38±0.43	10.2±1.05	1.84±0.18
	30	1.19±0.49	0.53±0.11	11.3±1.32	4.17±0.44	0.88±0.07
	60	0.64±0.13	0.28±0.04	14.1±0.55	3.25±0.27	1.38±0.46

Data are expressed as mean±SD (n=4 at each time point)

Kruskal–Wallis test). AD patients additionally had significantly lower mean MMSE scores than those with MCI ($P<$ 0.05, Kruskal–Wallis test). No toxic events were observed in the current clinical trial. The SUV-TACs from [^{18}F]FACT-PET in AD patients and normal control subjects are shown in Fig. 4. Both groups showed rapid entry of [^{18}F]FACT into the neocortex and cerebellum. In the AD patients, the temporal cortex, known to contain high concentrations of fibrillar amyloid plaques in AD, showed retention of [^{18}F] FACT during the later time points compared with the cerebellum (Fig. 4a). In contrast, TACs in the temporal cortex and the cerebellum were nearly identical in normal subjects (Fig. 4b). The subcortical white matter regions showed relatively lower entry and slower clearance than gray matter areas, but no difference in TACs between AD patients and normal controls.

SUVR in the lateral temporal cortex of AD patients was significantly higher over 10 min postinjection of [^{18}F]FACT than those of normal controls ($p<0.05$, Mann–Whitney U test) and reached maximum value at 30 to 40 min postinjection (Fig. 4c). Effect size between AD and normal controls showed the highest value at 30 to 40 min postinjection of [^{18}F]FACT (Table 3). The ratio of SUVR in AD to SUVR in normal controls became constant after

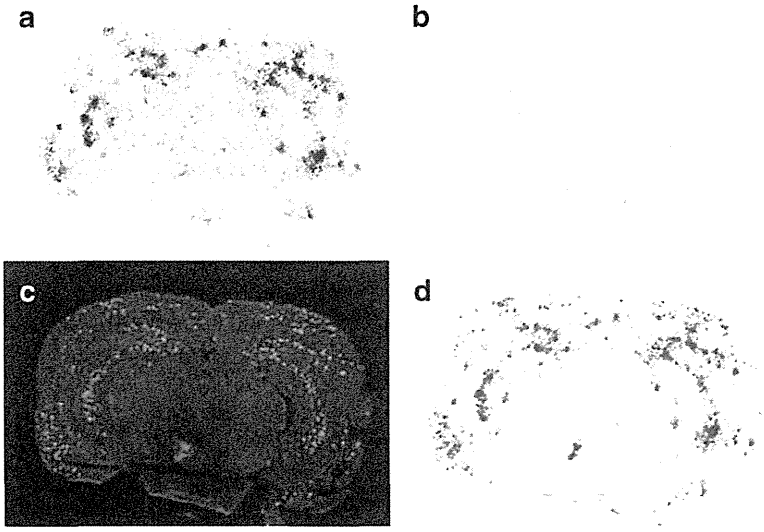

Fig. 3. *Ex vivo* autoradiograms of brain sections from APP transgenic (Tg) mouse (**a**) and wild type mouse (**b**). The brains were excised at 2 h after intravenous injection of [^{18}F]FACT. Aβ plaques in APP-Tg mouse brain were clearly stained with thioflavin-S (**c**). A merged image of **a** and **c** is shown in **d**.

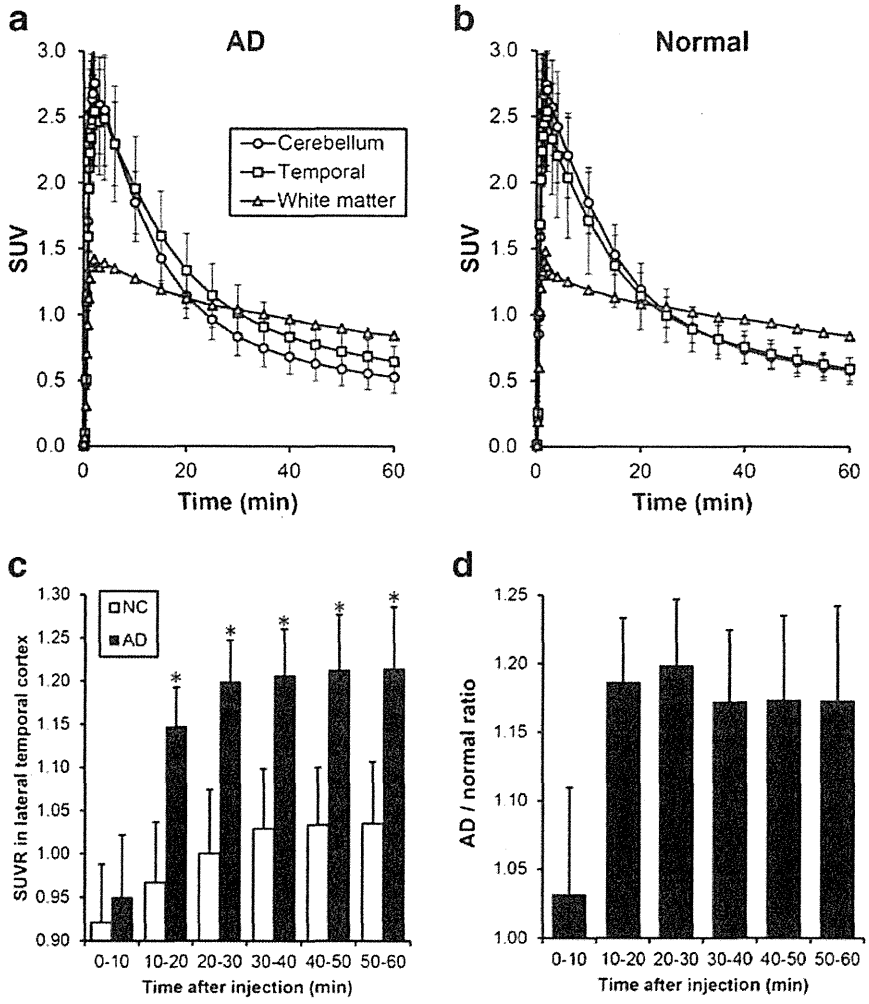

Fig. 4. Time activity data for [^{18}F]FACT PET in humans. Time activity curves of [^{18}F]FACT in ten AD patients (**a**) and ten normal controls (**b**) are shown. Each point represents the mean±standard deviations of data. Time course of [^{18}F]FACT SUVR in the lateral temporal cortex (**c**) and AD *vs* normal ratio of SUVR in the lateral temporal cortex (**d**) are also shown. *P<0.05 by the Mann–Whitney U test.

30 min (Fig. 4d). Based on these results, we selected summed dynamic images from 30 to 40 min for the ROI analysis of PET data.

SUVR images of [^{18}F]FACT for a normal control subject (a 60-year-old man, MMSE score 30) and an AD patient (70-year-old woman, MMSE score 17) are shown in Fig. 5a. Cortical retention of [^{18}F]FACT at 30 to 40 min postinjection was evident in the AD patient, as contrasted with the images of the normal control subject. This pattern of distribution was consistent with the distribution of [^{11}C]BF-227 at 30 to 40 min postinjection in the same subject and patient pair (Fig. 5a). The SUV-TACs from [^{18}F]FACT-PET were compared with those from [^{11}C]BF227-PET in the same AD patient (70-year-old woman, MMSE score 17). As shown in Fig. 5b, [^{18}F]FACT showed faster washout from both temporal cortex and cerebellum than [^{11}C]BF-227. The regional SUVR of [^{18}F]FACT at 30 to 40 min postinjection was compared with that of [^{11}C]BF-227 at the same time frame. SUVR values in the frontal, temporal, parietal, and occipital cortices of three subjects (two AD and one normal control) were used for this analysis. As shown in Fig. 5c, regional SUVR of [^{18}F]FACT were significantly correlated with that of [^{11}C]BF-227 (Pearson's r= 0.931, P<0.001) in these three subjects.

In the quantitative comparison of regional SUVR 30 to 40 min post-administration, the values for the frontal, lateral

Table 3. Time course of lateral temporal [^{18}F]FACT SUVR and effect size measures in ten normal controls and ten AD patients

Time (min)	Normal control	AD	Cohen's d
30–40	1.07±0.06	1.22±0.05*	2.67
40–50	1.08±0.06	1.23±0.06*	2.37
50–60	1.09±0.06	1.23±0.06*	2.34

*P<0.05 by the Mann–Whitney U test

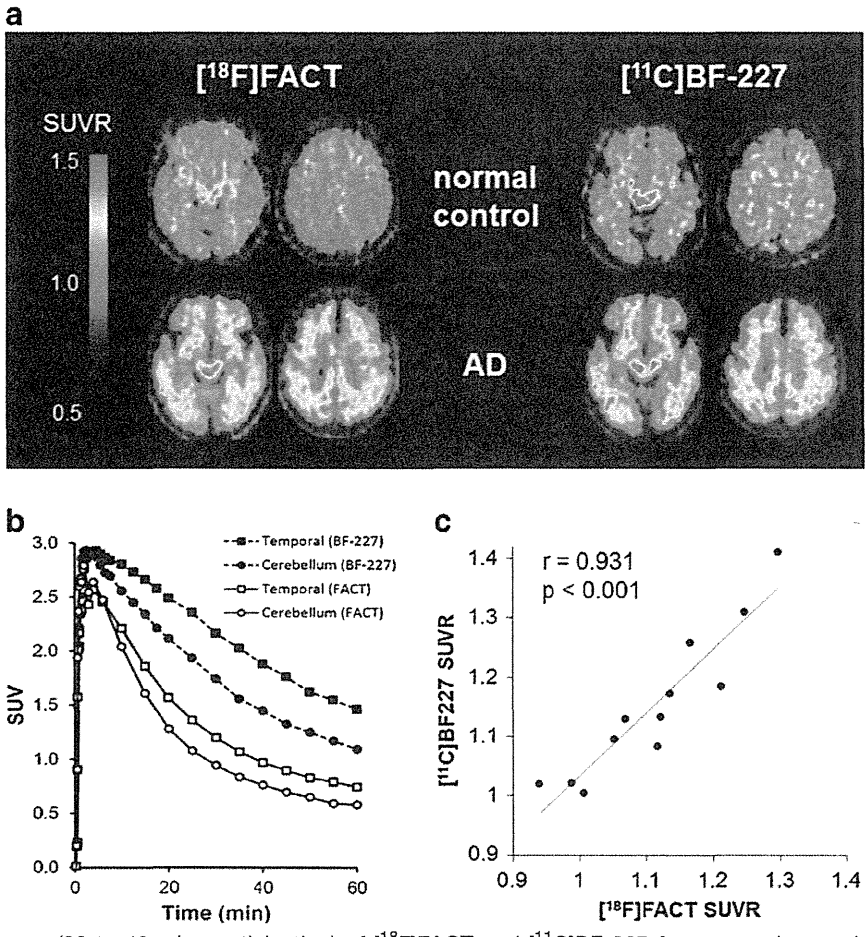

Fig. 5. **a** SUVR images (30 to 40 min postinjection) of [^{18}F]FACT and [^{11}C]BF-227 for a normal control subject (60-year-old man, MMSE score 30) and an AD patient (70-year-old woman, MMSE score 17). **b** Time activity curves of [^{18}F]FACT and [^{11}C]BF-227 in an AD patient (70-year-old woman, MMSE score 17). **c** Significant correlation between regional SUVR of [^{18}F]FACT and [^{11}C]BF-227 in two AD (70-year-old woman (MMSE score 17) and 79-year-old man (MMSE score 20)) and one normal control (60-year-old man, MMSE score 30) subjects (Pearson's r=0.931, P<0.001).

temporal, parietal, occipital, and anterior and posterior cingulate cortices were significantly greater in AD patients than in the normal controls (Table 4). In addition, the SUVRs for the lateral temporal, parietal, occipital, and anterior and posterior cingulate cortices were significantly greater in AD patients than in those with MCI. As shown in Fig. 6, averaged neocortical SUVR was also significantly greater in AD patients than in normal control subjects and MCI (P<0.05, Kruskal–Wallis test). MCI patients additionally showed significantly greater SUVR in the lateral temporal and frontal cortices than normal subjects, but not significant in other brain regions (P<0.05, Kruskal–Wallis

Table 4. Regional SUVR (30 to 40 min postinjection) and effect size measures of [^{18}F]FACT in ten normal controls and ten MCI and ten AD patients

	Normal control	MCI	AD	Cohen's d NC *vs.* AD
Frontal	1.00±0.10	1.09±0.04*	1.15±0.06*	1.82
Lateral temporal	1.05±0.08	1.13±0.06*	1.21±0.05*,**	2.40
Parietal	1.07±0.07	1.13±0.07	1.21±0.08*,**	1.86
Occipital	1.09±0.08	1.07±0.06	1.17±0.05*,**	1.20
Anterior cingulate	1.08±0.07	1.12±0.08	1.21±0.08*,**	1.73
Posterior cingulate	1.15±0.07	1.17±0.06	1.30±0.07*,**	2.14
Medial temporal	1.10±0.05	1.13±0.04	1.15±0.09	0.69
Striatum	1.31±0.11	1.30±0.06	1.35±0.12	0.35
Pons	1.55±0.15	1.57±0.10	1.54±0.09	0.08
White matter	1.50±0.21	1.47±0.11	1.52±0.13	0.12
Neocortex	1.04±0.07	1.12±0.05	1.19±0.05*,**	2.47

*P<0.05 (vs normal control group) and **P<0.05 (vs MCI group) by the Kruskal–Wallis test followed by Dunn's multiple comparison test

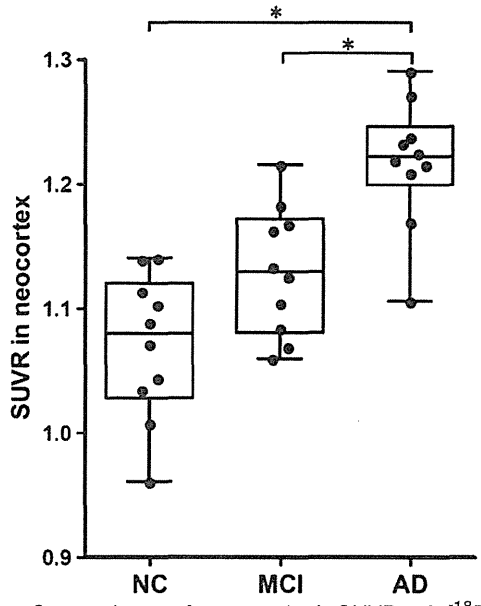

Fig. 6. Comparison of neocortical SUVR of [^{18}F]FACT among ten aged normal controls (NC) and ten mild cognitive impairment (MCI) and ten AD patients. The neocortical SUVRs are represented in a *box* and *whisker plot*. *P<0.05 by the Kruskal–Wallis test followed by Dunn's multiple comparison test.

test). The SUVR in the medial temporal cortex and striatum showed the tendency to be greater in AD patients, but this was not significant. The SUVR in the pons and white matter was nearly identical in AD, MCI, and normal subjects. Effect size value between AD and aged normal subjects was the highest in the lateral temporal cortex (2.40), followed by the posterior cingulate (2.14), parietal (1.86), frontal (1.82), and anterior cingulate (1.73) and occipital (1.20) cortices (Table 4).

Discussion

The current study demonstrated that [^{18}F]FACT PET can be used to detect AD pathology in AD patients and to confirm its absence in cognitively unimpaired elderly people. We previously reported the ability of [^{11}C]BF-227-PET to detect Aβ deposits in the brains of AD patients [15]. The current study has further demonstrated the binding preference of [^{18}F]FACT to dense Aβ plaques in the brains of AD patients. A similar pattern of tracer distribution was observed between [^{18}F]FACT and [^{11}C]BF-227 in AD patients, indicating that [^{18}F]FACT-PET could be substituted for [^{11}C]BF-227-PET for noninvasive detection of dense Aβ deposits in the brain of AD patients. The correlation of [^{18}F]FACT uptake *in vivo* and brain pathology at autopsy should be examined in the future. Our previous studies demonstrated the unique ability of [^{11}C]BF-227 to detect certain forms of prion and α-synuclein protein deposits [22, 23]. Further study will be required to validate the practical usefulness of [^{18}F]FACT-PET for noninvasive detection of these protein deposits.

When a neocortical [^{18}F]FACT SUVR of 1.145 (1.5 SD above control mean) was used as a cutoff, [^{18}F]FACT-PET scan achieved a sensitivity of 90 % (nine of ten) and a specificity of 100 % (ten of ten) in the discrimination between AD patients and normal subjects. In one exception, a 76-year-old female AD patient, MMSE score 24, showed no remarkable retention of [^{18}F]FACT in the neocortex. This is not surprising because approximately 10 to 20 % of patients diagnosed as probable AD reportedly fail to meet pathological criteria for AD at autopsy.

The amnestic subtype of MCI has a high risk of progression to dementia, and it may constitute a prodromal stage of AD [24]. Previous amyloid-PET studies demonstrated a substantial amount of neocortical tracer retention in 50 to 60 % of the MCI population, which is comparable to the level in AD patients [10, 17]. In our study, about half of the MCI patients had elevated neocortical [^{18}F]FACT retention, which was an intermediate level between the aged normal subjects and the AD patients. This finding is in accord with the previous neuropathological observation that the density of neuritic plaque increased as a function of increasing dementia severity [25]. The parent tracer [^{11}C]BF-227 showed neocortical retention to be a reliable indicator of disease progression in MCI subjects in our previous study [17, 19]. Therefore, PET imaging with [^{18}F]FACT is also expected to have a similar prognostic utility.

The amount of elevation of neocortical [^{18}F]FACT uptake in AD patients was approximately 14 to 15 %, far less than PiB and other ^{18}F-labeled amyloid-PET tracers. This is probably due to the relatively low binding affinity and B_{max} of this tracer with amyloid fibrils in comparison to that of PiB (K_d=1.02 nM, B_{max}=0.61) [26, 27]. There is considerable amount of tracer retention in the white matter, which reflects non-specific binding of the compound to myelin sheath. Because of modest specific binding of [^{18}F]FACT in the gray matter of AD patients, spillover from the white matter could reduce the sensitivity for detecting amyloid positive subjects. Use of early phase (30 to 40 min postinjection) images can compensate for this because the relatively stronger signals in the gray matter persist in this time interval. Partial volume correction may also be able to improve the discriminatory power of [^{18}F]FACT-PET by eliminating nonspecific signals in the white matter. Another method to improve the sensitivity for detecting specific signals in the brain is to create a statistical map by comparison with a normal control database [19].

One of advantages of [^{18}F]FACT over BF-227 is its rapid kinetic profile. [^{18}F]FACT showed faster washout from normal brain tissue than BF-227 (Fig. 5) probably because of the lower lipophilicity of FACT (LogP=1.99±0.02) as compared to BF-227 (LogP=2.29±0.02). The neocortical SUVR of [^{18}F]FACT reached a peak at 30 min post-administration. This characteristic would also contribute to reduced procedure and waiting times for PET scans.

Conclusion

We successfully developed a novel ^{18}F-labeled ethenylbenzoxazole derivative, [^{18}F]FACT, as a PET tracer for amyloid deposits. This tracer preferentially bound to dense Aβ plaques in AD brain sections, visualized cortical amyloid deposits in APP Tg mice, and demonstrated fast kinetics and significant retention of [^{18}F]FACT in sites with predilection for the deposition of dense amyloid plaques in AD patients during clinical PET imaging. [^{18}F]FACT PET distinctly distinguished AD patients from normal individuals. These findings suggest that [^{18}F]FACT may be usable for *in vivo* detection of dense Aβ plaques in AD brains.

Acknowledgments. This study was financially supported by the Special Coordination Funds for Promoting Science and Technology, the Health and Labour Sciences Research Grants for Translational research from Ministry of Health, Labour and Welfare, the Program for Promotion of Fundamental Studies in Health Science of the National Institute of Biomedical Innovation, and the Grant-in-Aid for Scientific Research (C) (20591432) from the Ministry of Education, Culture, Sports, Science and Technology of Japan. The authors appreciate the technical assistance of Dr. Shoichi Watanuki in the clinical PET studies.

Conflict of Interest. The authors declare they have no conflicts of interest.

References

1. McKhann GM, Knopman DS, Chertkow H et al (2011) The diagnosis of dementia due to Alzheimer's disease: recommendations from the National Institute on Aging—Alzheimer's Association workgroups on diagnostic guidelines for Alzheimer's disease. Alzheimers Dement 7:263–269
2. Kadir A, Nordberg A (2010) Target-specific PET probes for neurodegenerative disorders related to dementia. J Nucl Med Off Publ Soc Nucl Med 51:1418–1430
3. Furumoto S, Okamura N, Iwata R, Yanai K, Arai H, Kudo Y (2007) Recent advances in the development of amyloid imaging agents. Curr Top Med Chem 7:1773–1789
4. Okamura N, Fodero-Tavoletti MT, Kudo Y et al (2009) Advances in molecular imaging for the diagnosis of dementia. Expert Opin Med Diagn 3:705–716
5. Klunk WE, Engler H, Nordberg A et al (2004) Imaging brain amyloid in Alzheimer's disease with Pittsburgh Compound-B. Ann Neurol 55:306–319
6. Vandenberghe R, Van Laere K, Ivanoiu A et al (2010) ^{18}F-flutemetamol amyloid imaging in Alzheimer disease and mild cognitive impairment: a phase 2 trial. Ann Neurol 68:319–329
7. Barthel H, Gertz HJ, Dresel S et al (2011) Cerebral amyloid-beta PET with florbetaben (^{18}F) in patients with Alzheimer's disease and healthy controls: a multicentre phase 2 diagnostic study. Lancet Neurol 10:424–435
8. Clark CM, Schneider JA, Bedell BJ et al (2011) Use of florbetapir-PET for imaging beta-amyloid pathology. Jama 305:275–283
9. Jureus A, Swahn BM, Sandell J et al (2010) Characterization of AZD4694, a novel fluorinated Abeta plaque neuroimaging PET radioligand. J Neurochem 114:784–794
10. Rowe CC, Ng S, Ackermann U et al (2007) Imaging beta-amyloid burden in aging and dementia. Neurology 68:1718–1725
11. Hatashita S, Yamasaki H (2010) Clinically different stages of Alzheimer's disease associated by amyloid deposition with [^{11}C]-PIB PET imaging. J Alzheimer's Dis JAD 21:995–1003
12. Villemagne VL, Pike KE, Chetelat G et al (2011) Longitudinal assessment of Abeta and cognition in aging and Alzheimer disease. Ann Neurol 69:181–192
13. Dickson TC, Vickers JC (2001) The morphological phenotype of beta-amyloid plaques and associated neuritic changes in Alzheimer's disease. Neuroscience 105:99–107
14. Okamura N, Suemoto T, Shimadzu H et al (2004) Styrylbenzoxazole derivatives for *in vivo* imaging of amyloid plaques in the brain. J Neurosci 24:2535–2541
15. Kudo Y, Okamura N, Furumoto S et al (2007) 2-(2-[2-Dimethylaminothiazol-5-yl]ethenyl)-6- (2-[fluoro]ethoxy)benzoxazole: a novel PET agent for *in vivo* detection of dense amyloid plaques in Alzheimer's disease patients. J Nucl Med 48:553–561
16. Barthel H, Luthardt J, Becker G et al (2011) Individualized quantification of brain beta-amyloid burden: results of a proof of mechanism phase 0 florbetaben PET trial in patients with Alzheimer's disease and healthy controls. Eur J Nucl Med Mol Imaging 38:1702–1714
17. Waragai M, Okamura N, Furukawa K et al (2009) Comparison study of amyloid PET and voxel-based morphometry analysis in mild cognitive impairment and Alzheimer's disease. J Neurol Sci 285:100–108
18. Kudo Y, Furumoto S, Okamura N (2010) Benzoxazole derivatives. US Patent Application 2010/0021385
19. Shao H, Okamura N, Sugi K et al (2010) Voxel-based analysis of amyloid positron emission tomography probe [^{11}C]BF-227 uptake in mild cognitive impairment and Alzheimer's disease. Dement Geriatr Cogn Disord 30:101–111
20. McKhann G, Drachman D, Folstein M, Katzman R, Price D, Stadlan EM (1984) Clinical diagnosis of Alzheimer's disease: report of the NINCDS-ADRDA Work Group under the auspices of Department of Health and Human Services Task Force on Alzheimer's Disease. Neurology 34:939–944
21. Petersen RC, Smith GE, Waring SC, Ivnik RJ, Tangalos EG, Kokmen E (1999) Mild cognitive impairment: clinical characterization and outcome. Arch Neurol 56:303–308
22. Okamura N, Shiga Y, Furumoto S et al (2009) *In vivo* detection of prion amyloid plaques using [^{11}C]BF-227 PET. Eur J Nucl Med Mol Imaging 37:934–941
23. Kikuchi A, Takeda A, Okamura N et al (2010) *In vivo* visualization of alpha-synuclein deposition by carbon-11-labelled 2-[2-(2-dimethylaminothiazol-5-yl)ethenyl]-6-[2-(fluoro)ethoxy]benzoxazole positron emission tomography in multiple system atrophy. Brain J Neurol 133:1772–1778
24. Gauthier S, Reisberg B, Zaudig M et al (2006) Mild cognitive impairment. Lancet 367:1262–1270
25. Haroutunian V, Perl DP, Purohit DP et al (1998) Regional distribution of neuritic plaques in the nondemented elderly and subjects with very mild Alzheimer disease. Arch Neurol 55:1185–1191
26. Fodero-Tavoletti MT, Mulligan RS, Okamura N et al (2009) *In vitro* characterisation of BF227 binding to alpha-synuclein/Lewy bodies. Eur J Pharmacol 617:54–58
27. Fodero-Tavoletti MT, Smith DP, McLean CA et al (2007) *In vitro* characterization of Pittsburgh compound-B binding to Lewy bodies. J Neurosci Off J Soc Neurosci 27:10365–10371

Jpn J Radiol (2014) 32:138–144
DOI 10.1007/s11604-013-0276-7

ORIGINAL ARTICLE

Analysis of early phase [^{11}C]BF-227 PET, and its application for anatomical standardization of late-phase images for 3D-SSP analysis

Tomohiro Kaneta · Nobuyuki Okamura · Akira Arai · Kentaro Takanami · Katsutoshi Furukawa · Manabu Tashiro · Shozo Furumoto · Ren Iwata · Shoki Takahashi · Hiroyuki Arai · Kazuhiko Yanai · Yukitsuka Kudo

Received: 14 August 2013 / Accepted: 22 December 2013 / Published online: 10 January 2014

Abstract
Purpose To examine the usefulness of the early phase [^{11}C]BF-227 positron emission tomography (PET) for (1) conferring additional diagnostic value by providing perfusion-like information and (2) obtaining the appropriate anatomical standardization (AS) using three-dimensional stereotactic surface projection (3D-SSP) method.
Methods This study included 20 mild cognitive impairment (MCI), 19 Alzheimer's disease (AD), and 17 normal cognitive (NC) subjects. Early- and late-phase BF-227 PET images were obtained 0–10 and 40–60 min after the injection, respectively. AS for late-phase BF-227 images were performed by 2 methods: (1) method A, for AS of late-phase BF-227 images using ^{8}F-fluorodeoxyglucose (FDG) images of the same subject and (2) method B, for AS of late-phase BF-227 images using early phase BF-227 images.
Results Method B was successfully used for AS in all cases. The Z score maps of 3D-SSP analyses of FDG PET and early phase BF-227 PET for AD and MCI groups showed a typical AD-like pattern. Regional analyses revealed that the early phase BF-227 PET showed significant differences between AD and NC, and MCI and NC.
Conclusion The early phase BF-227 PET images showed significant abnormal findings for the AD and MCI groups. AS of late-phase BF-227 images using early phase BF-227 images were successful, and enabled appropriate 3D-SSP analyses.

Keywords Amyloid imaging · Early phase · BF-227 · Alzheimer's disease · 3D-SSP

T. Kaneta (✉) · A. Arai · K. Takanami · S. Takahashi
Department of Diagnostic Radiology, Tohoku University, 1-1 Seiryomachi, Aobaku, Sendai 980-8574, Japan
e-mail: kaneta@rad.med.tohoku.ac.jp

N. Okamura · K. Yanai
Department of Pharmacology, Tohoku University Graduate School of Medicine, 4-1 Seiryomachi, Aobaku, Sendai 980-8575, Japan

K. Furukawa
Division of Brain Sciences, Department of Geriatrics and Gerontology, Institute of Development, Aging and Cancer, Tohoku University, 4-1 Seiryomachi, Aobaku, Sendai 980-8498, Japan

M. Tashiro · H. Arai
Division of Cyclotron Nuclear Medicine, Cyclotron and Radioisotope Center, Tohoku University, 6-3 Aoba, Aramaki, Aoba-ku, Sendai, Miyagi 980-8578, Japan

S. Furumoto · R. Iwata
Division of Radiopharmaceutical Chemistry, Cyclotron and Radioisotope Center, Tohoku University, 6-3 Aoba, Aramaki, Aoba-ku, Sendai, Miyagi 980-8578, Japan

Y. Kudo
Department of NeuroImaging Research, Innovation New Biomedical Engineering Center, Tohoku University, 4-1 Seiryomachi, Aobaku, Sendai 980-8498, Japan

Introduction

Three-dimensional stereotactic surface projection (3D-SSP) analysis [1, 2] has been widely used in voxel-based statistical analyses of ^{18}F-fluorodeoxyglucose (FDG) positron emission tomography (PET) and brain perfusion single-photon emission computed tomography (SPECT) data. In 3D-SSP analyses, anatomical standardization (AS) is performed using a brain template created from FDG PET data (the FDG template) [2], even for analyses of brain perfusion SPECT. It has been thought that 3D-SSP is

unsusceptible to the tracer distribution because of the usage of both a template and landmarks. Thus, 3D-SSP does not necessarily require individual templates for each tracer [3]. However, in analyses of amyloid PET, 3D-SSP analyses can sometimes cause errors because of inadequate AS, which might be caused by the large differences in distribution between FDG and amyloid tracers. Thus, a modified method of 3D-SSP analysis for amyloid PET using FDG PET has been developed [4]. In this method, an FDG PET scan of the same subject was used to calculate the parameters for AS, and these parameters were subsequently used for the AS of an amyloid PET scan. Recently, a few researchers focused on early phase amyloid PET scans using ^{11}C-Pittsburgh compound B (PiB) [5] and ^{18}F-florbetapir [6], and reported that early phase amyloid PET was potentially useful in providing complementary perfusion- or FDG-like information. In this study, we examined the suitability of early phase amyloid PET using ^{11}C-labeled 2-(2-[2-dimethylaminothiazol-5-yl]ethenyl)-6-(2-[fluoro]ethoxy)benzoxazole (BF-227) [7–9] for (1) conferring additional diagnostic value by providing perfusion-like information and (2) obtaining the appropriate AS in 3D-SSP analyses.

Methods

For the present study, we recruited 20 subjects with amnestic mild cognitive impairment (MCI), 19 subjects with Alzheimer's disease (AD), and 17 normal cognitive (NC) subjects. The diagnosis of AD and MCI was made according to the National Institute of Neurological and Communicative Diseases and Stroke/Alzheimer's Disease and Related Disorders Association criteria. The demographic information of the subjects is shown in Table 1. In this study, the subjects were overlapped with the previous study [4]. The NC group was recruited from among volunteers, none of whom were prescribed centrally acting medication, had cognitive impairment, or had cerebrovascular lesions identified on MRI. The study protocol was approved by the Committee on Clinical Investigation at our institution. After receiving information about the study, written informed consent was obtained from all participants.

Table 1 Demographic detail of the subjects in this study

	N	Gender	Age	MMSE
AD	19	M/F = 5/14	73.7 ± 7.0	20.0 ± 3.5
MCI	20	M/F = 10/10	76.6 ± 4.7	25.5 ± 2.3
NC	17	M/F = 8/9	67.0 ± 4.1	29.9 ± 0.3

AD Alzheimer's disease, *MCI* mild cognitive impairment, *NC* normal cognitive subject

All subjects underwent PET with both FDG and BF-227 within 3 months. All patients were clinically stable between the visits. BF-227 and its *N*-demethylated derivative (a precursor of BF-227) were custom-synthesized by Tanabe R&D Service Co., Japan. BF-227 was synthesized from its precursor by *N*-methylation in dimethyl sulfoxide using [^{11}C]methyl triflate. Both FDG and BF-227 PET were performed using a PET SET-2400W scanner (Shimadzu Inc., Japan) with a spatial resolution of 4 mm (transaxial) and 4.5 mm (axial) at full-width half-maximum (FWHM) in the center of the field of view. For attenuation correction, a transmission scan was performed using ^{68}Ge/Ga sources for 7 min. After intravenous bolus injection of 211–366 MBq of BF-227 (a volume of 2 cc) dynamic PET data were obtained for 60 min (23 sequential scans: 5 scans × 30 s, 5 scans × 60 s, 5 scans × 150 s, and 8 scans × 300 s) with each subject's eyes closed. The subject's head was fixed with a band. Head motion was monitored with a camera and an alarm. The data obtained 0–10 and 40–60 min after injection were used as early- and late-phase BF-227 PET data, respectively. For FDG PET, subjects were scanned in a quiet and dimly lit room with their eyes closed after fasting for at least 4 h. An emission scan of 15 min was started 45 min after an intravenous injection of approximately 370 MBq of FDG. The emission data were corrected for tissue attenuation based on the transmission data. These data were used for the calculation of standardized uptake value (SUV), a tissue radioactivity concentration normalized by injected dose and body weight.

Anatomical standardization of BF-227 images

Two kinds of AS for late-phase BF-227 images were performed: (1) method A, for AS of late-phase BF-227 images using FDG images of the same subject and (2) method B, for AS of late-phase BF-227 images using early phase BF-227 images. The specific procedures are described below. First, the FDG images and early phase BF-227 images were subjected to AS using an FDG template. Late-phase BF-227 images were then registered to the FDG images (method A) and to early phase BF-227 images (method B). AS was performed using transformation parameters calculated for the AS of the corresponding FDG images (method A) and for the early phase BF-227 images (method B). We used the software library Neurostat (University of Washington, Seattle, WA, USA) for neurological and biomedical image analyses. The precise programming methods have been described in [4]. The distortion of images after anatomical standardization was evaluated by reference to sample images with mild and severe distortion in [4].

Analysis

For voxel-based comparisons with normal subjects, normal databases were created by averaging the images from the NC group after AS by methods A and B, individually. The 3D-SSP Z-score map images were normalized to those of the cerebellum for late BF-227 images and to those of the pons for early BF-227 images and FDG images, and were shown to be within a range of 1–5 of the Z-score.

For voxel-based two-sample comparisons, a *t*-test was applied. Z-scores were calculated using the "ssp2tz" program in Neurostat. The 3D-SSP Z-map images were shown to be within a range of 1–5 of the Z-score.

Regional SUV values were extracted from cortical gray matter to the surface of the template by the 3D-SSP method, and were normalized by the value from the pons (nSUV). The values were calculated for the frontal, parietal, temporal, occipital and posterior cingulated cortices (PCC) using the "sspvoiclassic" program in Neurostat. The right and left lobes of each subject were analyzed evenly. For multiple comparisons between the 3 groups, we applied a Tukey-Kramer test using JMP Pro 9 (SAS Institute, NC, USA). For comparisons between the results from method A and B, we applied a paired *t*-test using Excel (Microsoft, WA, USA). Statistical significance was defined as $p < 0.05$.

Results

Comparison of FDG and early phase BF-227 PET

Case presentation

A 75-year-old man diagnosed with AD scored 19 on the mini-mental state examination (MMSE). As seen in Fig. 1, cross-sectional images and 3D-SSP results from FDG PET showed a typical AD-like pattern, which was characterized by decreased uptake in the PCC and parietal lobes. On the other hand, the cross-sectional images and 3D-SSP results of early phase BF-227 PET also showed a typical AD-like pattern, but the findings were less clear than those from FDG PET.

Group comparisons of FDG PET and early phase BF-227 PET

Figure 2 shows the Z-score maps from 3D-SSP analyses of FDG PET and early phase BF-227 PET, comparing the AD and NC groups and the MCI and NC groups. In both comparisons, FDG PET showed a typical AD-like pattern, which was characterized by decreased uptake in the PCC, parietal lobes, frontal lobes, and temporal lobes, but sparing the primary sensorimotor areas. Early phase BF-227 PET also showed a similar pattern, but the Z-scores were slightly lower than those from FDG PET.

Regional analyses

The regional analyses revealed that the mean nSUV values of FDG PET for the AD, MCI, and NC groups were in the ranges of 1.09–1.28, 1.14–1.27, and 1.28–1.42, respectively, whereas those of early phase BF-227 PET were found to be in the ranges of 0.93–1.06, 0.96–1.06, and 1.02–1.17, respectively. FDG PET showed significant differences between the AD and NC groups and between the MCI and NC groups in the parietal, temporal, and frontal lobes, and in the PCC (Fig. 3a). Early phase BF-227 PET also showed significant differences between them, with the exception of comparisons between the MCI and NC groups at the temporal lobes (Fig. 3b).

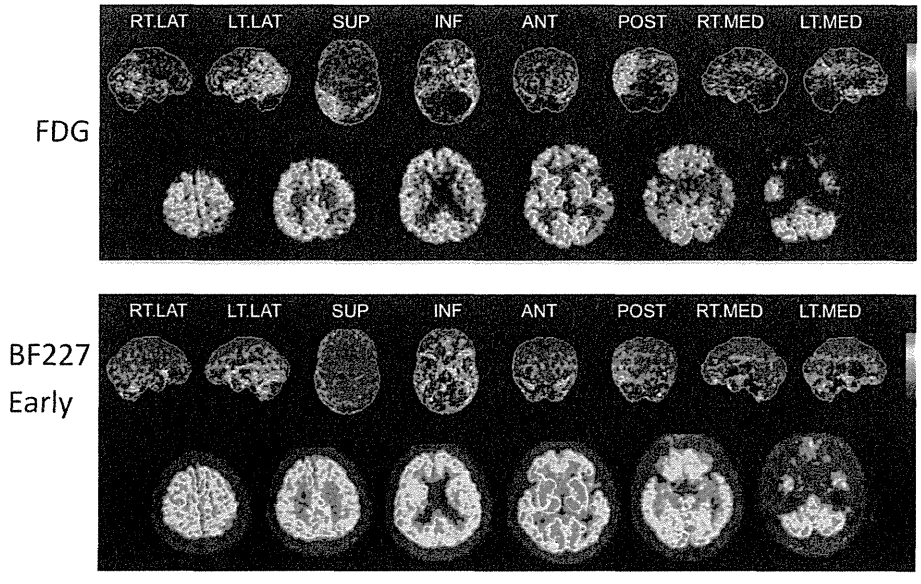

Fig. 1 Images of a 75-year-old man with AD. The mini-mental state examination (MMSE) score was 19. *Upper row* 3D-SSP results and cross-sectional images of FDG PET. *Lower row* 3D-SSP results and cross-sectional images of early phase BF-227 PET

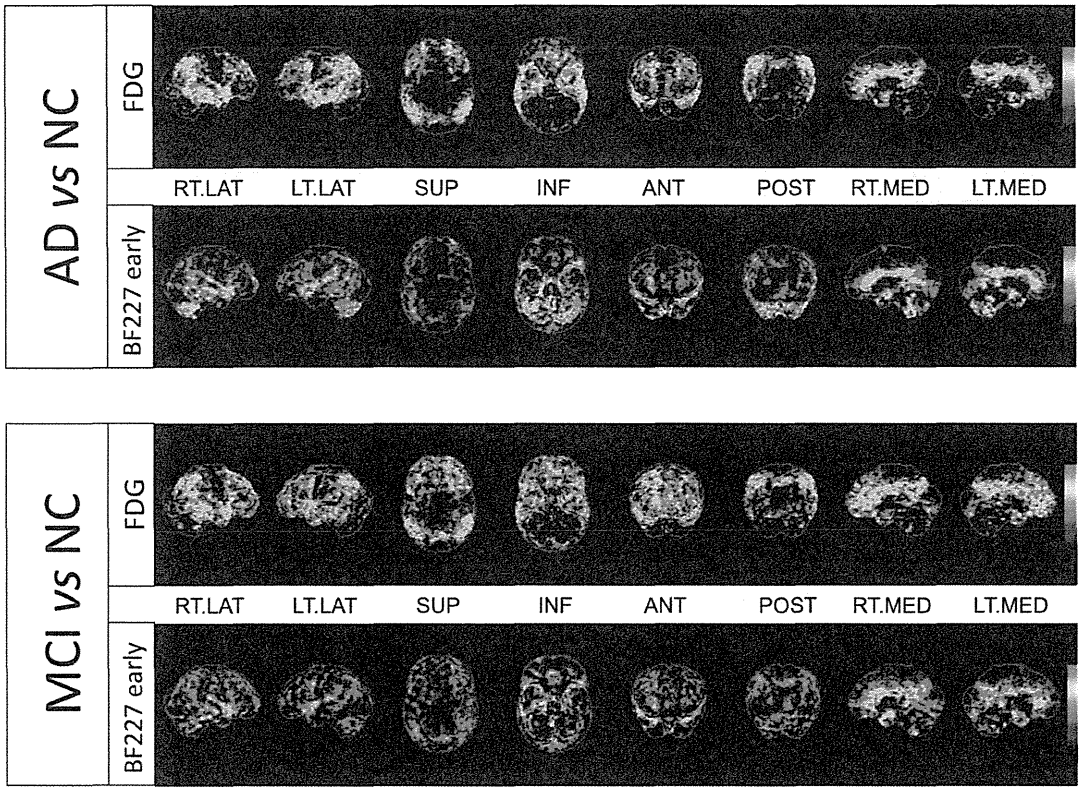

Fig. 2 Z score maps of 3D-SSP analyses of FDG PET and early phase BF-227 PET, comparing AD and NC groups (*upper*) and MCI and NC groups (*lower*)

Changes after anatomical standardization of late-phase BF-227 images

As reported previously [4], method A ("method 2" in the previous paper) was successfully used to perform AS in all but 2 cases. These 2 cases included 1 involving scan failure and another with an error in the registration of the BF-227 image to the FDG image; this necessitated their exclusion from subsequent analyses.

On the other hand, method B, which is a newly modified method using early phase BF-227 PET, was successfully used to perform AS in all cases.

Figure 4 shows sample images after AS from a 60-year-old female NC subject. Figure 4a–c demonstrate the images after AS using late-phase BF-227 images, method A, and method B, respectively. Figure 4a shows obvious distortion, especially in the frontal lobes, but Fig. 4b and c show successful AS.

Comparisons of the late-phase BF-227 images analyzed by methods A and B

Figure 5 shows the Z-score maps of late-phase BF-227 images after the 3D-SSP analyses using methods A and B, comparing the AD and NC groups and the MCI and NC groups. A comparison of the AD and NC groups using methods A and B showed almost the same distribution and values in the Z-score maps. A comparison of the MCI and NC groups using methods A and B showed almost the same distribution, but method B resulted in slightly lower values than method A. Table 2 shows the differences of nSUV derived from method A and B at the parietal, frontal, temporal and occipital lobe. There were no significant differences at the parietal, frontal and occipital lobe. But, there was a significant difference at the temporal lobe ($p < 0.01$).

Discussion

Early phase BF-227 images obtained in our study were totally different from late-phase images and more perfusion-like, and were compatible with those obtained in previous studies using PiB [5] and ^{18}F-florbetapir [6]. These amyloid PET tracers are highly lipophilic, and possibly have a higher first-pass influx rate (K_1) [10]. Thus, images obtained during early timeframes contain information related to K_1 [11]. These values of K_1 have also

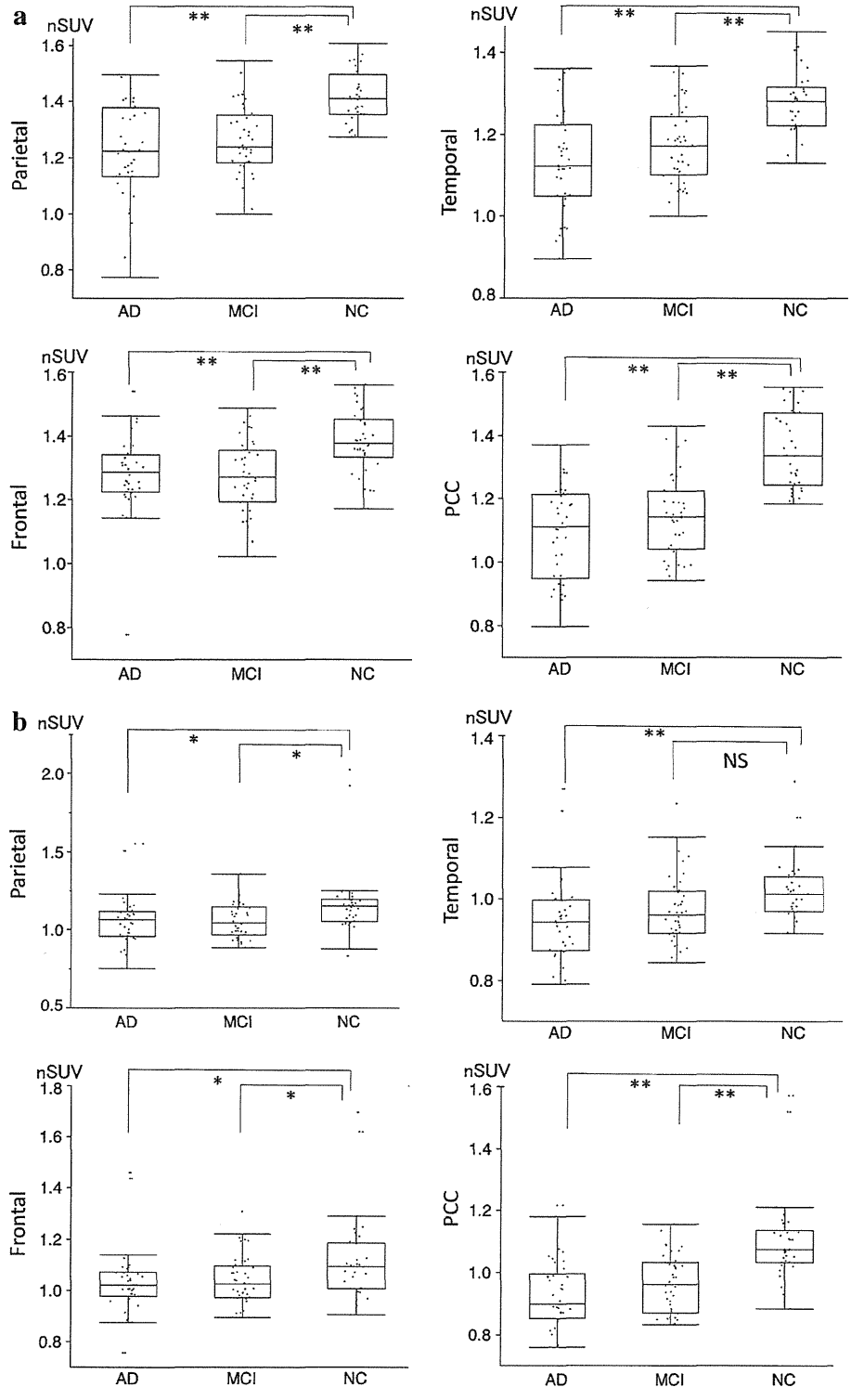

Fig. 3 Regional analyses of FDG PET (**a**) and early phase BF-227 PET (**b**) among AD, MCI, and NC groups. The values normalized to the pons were evaluated at the parietal, temporal, and frontal lobes and the posterior cingulated cortices (PCC). The box and whisker plots represent median (*horizontal line*), 1st quartile (*lower limit of box*), 3rd quartile (*upper limit of box*), and minimum and maximum values, respectively. $^{**}p < 0.01$, $^{*}p < 0.05$, *NS* not significant

been found to represent unidirectional influx of the tracer into the brain and are related to perfusion [12]. In addition, correlations between metabolism and cerebral perfusion have been long established in healthy older individuals and in those with degenerative dementias, likely because reduced metabolic demand is related to reduced perfusion [13]. Thus, it is not surprising that early PET frames of amyloid tracers show perfusion-like or FDG-like images.

Hereinafter, we discuss the benefits of obtaining these images.

Our results showed that the appropriate AS of 3D-SSP was successfully performed using early phase BF-227 images. Previously, we used FDG images for the AS of 3D-SSP because 3D-SSP uses an FDG template [1, 2]. The images obtained from early phase BF-227 PET were successfully transformed to the FDG template during the AS of 3D-SSP. Our modified 3D-SSP methods rely on the accurate co-registration of the images of the same subject using linear transformations, such as rotation, stretching, shrinking, and shearing. Non-linear warping is not necessary for the co-registration of images from the same subject. Thus, the co-registration of FDG and BF-227 images, or that of early- and late-phase BF-227 images can be performed accurately. However, method A produced an error in the registration of the BF-227 image to the FDG image in 1 case, while method B did not produce any errors. This can be explained by the smaller degree of dislocation between early- and late-phase BF-227 scans than between the FDG and BF-227 scans. Early- and late-phase BF-227 scans were performed on the same day without repositioning the patients' bodies, whereas

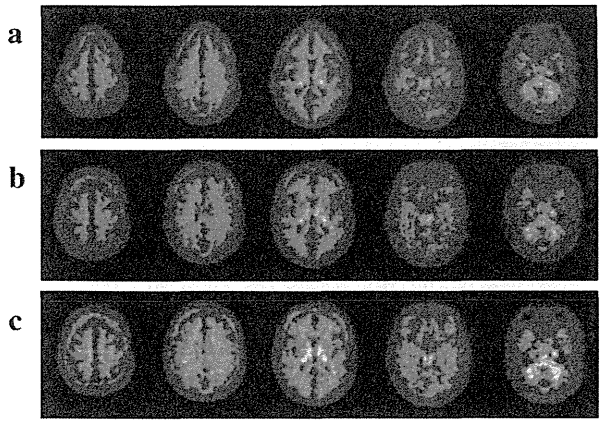

Fig. 4 Sample images after AS of 60-year-old female NC subject. **a–c** demonstrate the images after AS using late-phase BF-227 images, method A, and method B, respectively

Table 2 Comparison of nSUV between the results of methods A and B

	Parietal	Temporal*	Frontal	Occipital
Method A	1.03 ± 0.01	1.06 ± 0.01	1.05 ± 0.01	1.07 ± 0.01
Method B	1.02 ± 0.01	1.04 ± 0.01	1.03 ± 0.01	1.07 ± 0.01

* $p < 0.01$

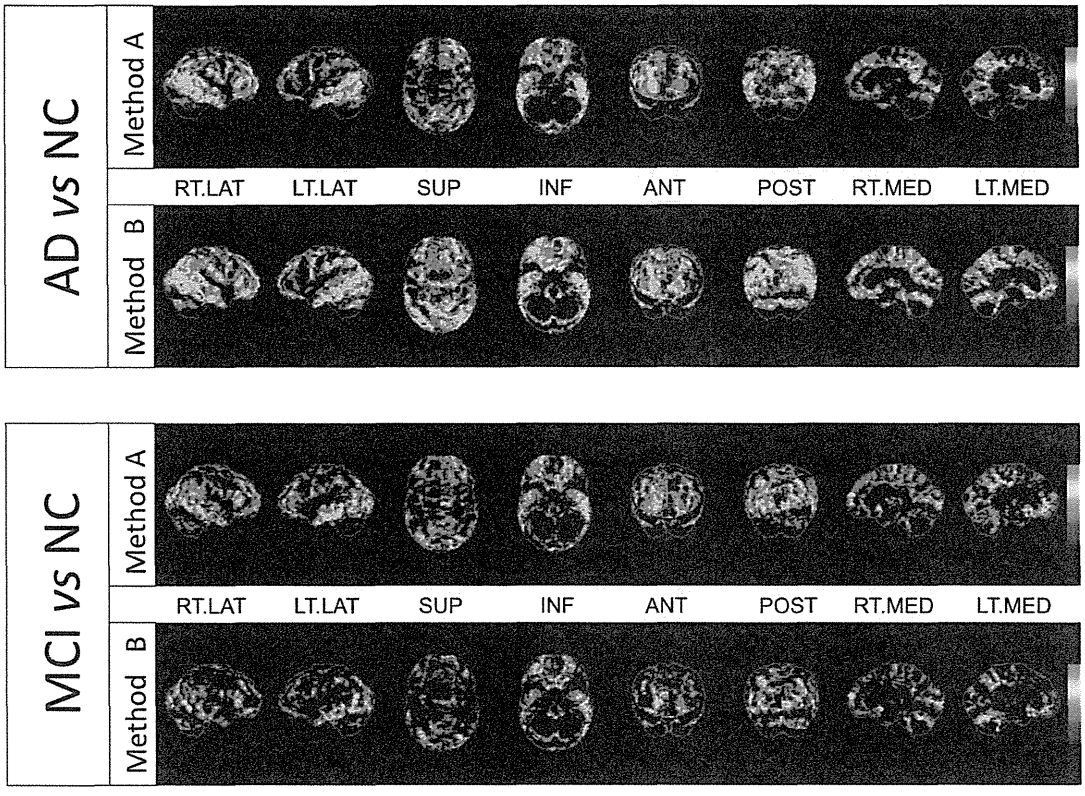

Fig. 5 Z score maps of late-phase BF-227 images after 3D-SSP analyses comparing AD and NC groups (*upper*) and MCI and NC groups (*lower*) by methods A and B

the FDG and BF-227 scans were performed with an interval between of several days to a few months. Thus, it may be preferable to use method B to obtain an appropriate AS. In addition, FDG images may not necessarily be required for the 3D-SSP analysis of amyloid PET. This could reduce the need for an additional patient visit or higher exposure to the radioactivity of FDG imaging. Furthermore, no significant differences were observed between the results of 3D-SSP performed by methods A and B. As shown in Fig. 5, no significant differences were found between methods A and B in the AD group versus the NC group. For the MCI group versus the NC group, the abnormal findings obtained with method B appear slightly smaller in the Z-score maps than those obtained with method A. Table 2 showed a significant difference in nSUV derived from methods A and B at the temporal lobe only, but not at the parietal, frontal and occipital lobes. The reason for such differences remains unknown. However, it might be caused by the difference of the tracer distribution around the temporal lobe between FDG and early phase BF-227, or the sampling method of "sspvoiclassic" in Neurostat.

Next, our results showed that early phase BF-227 images were significantly different between the AD and NC groups and between the MCI and NC groups in the parietal, temporal, and frontal lobes, and in the posterior cingulate cortices in all cases, except between the MCI and NC groups in the temporal lobes. These results are similar to those obtained with the FDG images, and suggest that early phase BF-227 images have equivalent diagnostic power to FDG images in terms of group comparisons between AD and NC, and MCI and NC. However, the visual evaluation of early phase BF-227 images may be still difficult for individual diagnosis. As shown in Figs. 1 and 2, the FDG PET findings were clearer than those from early phase BF-227 PET. One of the main reasons might be the lack of optimization of early phase scanning time. From the results of time activity curves of BF-227 [8], AD patients showed a significant difference over 10 min in the cortical areas and cerebellum, but normal subjects showed no significant differences. Thus, we set the early phase as a timeframe of 0–10 min, which seemed not to be amyloid-specific, but rather perfusion-like. However, optimization of scanning time may improve the image quality and the adherence to perfusion or FDG images. In previous studies that compared various time frames, scanning times of 1–8 min for PiB [5] and 1–6 min for AV-45 [6] were thought to be optimal for early phase imaging. As another limitation of this study, significant differences in age were seen between AD and NC, and MCI and NC groups. This study mainly focused on the methodological aspect, however, age-matched NC subjects should be compared in the clinical setting.

In conclusion, early phase BF-227 images were perfusion-like, and showed significant differences between the AD and NC groups, and between the MCI and NC groups. In addition, we developed a modified method for 3D-SSP analyses using early phase BF-227 PET. The results of this study demonstrate that the use of early phase images may improve the utility of amyloid PET for further dementia studies.

Acknowledgments This work was supported by JSPS KAKENHI Grant Number 24591745.

Conflict of interest The authors declare that they have no conflict of interest.

References

1. Minoshima S, Koeppe RA, Frey KA, Kuhl DE. Anatomic standardization: linear scaling and nonlinear warping of functional brain images. J Nucl Med. 1994;35:1528–37.
2. Minoshima S, Frey KA, Koeppe RA, Foster NL, Kuhl DE. A diagnostic approach in Alzheimer's disease using three-dimensional stereotactic surface projections of fluorine-18-FDG PET. J Nucl Med. 1995;36:1238–48.
3. Yamamoto Y, Onoguchi M. Statistical image analysis method to use for cerebral blood flow SPECT examination: difference and matters that require attention of processing of eZIS and iSSP. Nihon Hoshasen Gijutsu Gakkai Zasshi. 2011;67:718–27 (Japanese).
4. Kaneta T, Okamura N, Minoshima S, Furukawa K, Tashiro M, Furumoto S, et al. A modified method of 3D-SSP analysis for amyloid PET imaging using [^{11}C]BF-227. Ann Nucl Med. 2011;25:732–9.
5. Rostomian AH, Madison C, Rabinovici GD, Jagust WJ. Early 11C-PIB frames and 18F-FDG PET measures are comparable: a study validated in a cohort of AD and FTLD patients. J Nucl Med. 2011;52:173–9.
6. Hsiao IT, Huang CC, Hsieh CJ, Hsu WC, Wey SP, Yen TC, et al. Correlation of early-phase 18F-florbetapir (AV-45/Amyvid) PET images to FDG images: preliminary studies. Eur J Nucl Med Mol Imaging. 2012;39:613–20.
7. Kudo Y. Development of amyloid imaging PET probes for an early diagnosis of Alzheimer's disease. Minim Invasive Ther Allied Technol. 2006;15:209–13.
8. Kudo Y, Okamura N, Furumoto S, Tashiro M, Furukawa K, Maruyama M, et al. 2-(2-[2-Dimethylaminothiazol-5-yl]ethenyl)-6-(2-[fluoro]ethoxy)benzoxazole: a novel PET agent for in vivo detection of dense amyloid plaques in Alzheimer's disease patients. J Nucl Med. 2007;48:553–61.
9. Furumoto S, Okamura N, Iwata R, Yanai K, Arai H, Kudo Y. Recent advances in the development of amyloid imaging agents. Curr Top Med Chem. 2007;7:1773–89.
10. Treyer V, Streffer J, Wyss MT, Bettio A, Ametamey SM, Fischer U, et al. Evaluation of the metabotropic glutamate receptor subtype 5 using PET and 11C-ABP688: assessment of methods. J Nucl Med. 2007;48:1207–15.
11. Koeppe RA, Gilman S, Joshi A, Liu S, Little R, Junck L, et al. 11C-DTBZ and 18F-FDG PET measures in differentiating dementias. J Nucl Med. 2005;46:936–44.
12. Blomquist G, Engler H, Nordberg A, Ringheim A, Wall A, Forsberg A, et al. Unidirectional influx and net accumulation of PIB. Open Neuroimaging J. 2008;2:114–25.
13. Silverman DH. Brain ^{18}F-FDG PET in the diagnosis of neurodegenerative dementias: comparison with perfusion SPECT and with clinical evaluations lacking nuclear imaging. J Nucl Med. 2004;45:594–607.

Novel ^{18}F-Labeled Arylquinoline Derivatives for Noninvasive Imaging of Tau Pathology in Alzheimer Disease

Nobuyuki Okamura[1], Shozo Furumoto[1,2], Ryuichi Harada[1], Tetsuro Tago[2], Takeo Yoshikawa[1], Michelle Fodero-Tavoletti[3], Rachel S. Mulligan[4], Victor L. Villemagne[4], Hiroyasu Akatsu[5], Takayuki Yamamoto[5], Hiroyuki Arai[6], Ren Iwata[2], Kazuhiko Yanai[1], and Yukitsuka Kudo[7]

[1]Department of Pharmacology, Tohoku University School of Medicine, Sendai, Japan; [2]Division of Radiopharmaceutical Chemistry, Cyclotron and Radioisotope Center, Tohoku University, Sendai, Japan; [3]Department of Pathology, University of Melbourne, Victoria, Australia; [4]Department of Nuclear Medicine and Centre for PET, Austin Health, Melbourne, Victoria, Australia; [5]Choju Medical Institute, Fukushimura Hospital, Toyohashi, Japan; [6]Department of Geriatrics and Gerontology, Institute of Development, Aging and Cancer, Tohoku University, Sendai, Japan; and [7]Clinical Research, Innovation and Education Center, Tohoku University Hospital, Sendai, Japan

Neurofibrillary tangles in Alzheimer disease (AD) brains are composed of the microtubule-associated protein tau. Noninvasive monitoring of tau protein aggregates in the living brain will provide useful information regarding tau pathophysiology in AD. However, no PET probes are currently available for selective detection of tau pathology in AD. We have previously reported ^{18}F-labeled THK-523 (^{18}F-6-(2-fluoroethoxy)-2-(4-aminophenyl)quinoline) as a tau imaging radiotracer candidate for PET. After compound optimization, we developed novel ^{18}F-labeled arylquinoline derivatives, ^{18}F-THK-5105 and ^{18}F-THK-5117, for use as tau imaging PET tracers. **Methods:** ^{18}F-labeled compounds were prepared from the corresponding tosylated precursors. The binding affinity of compounds to synthetic tau aggregates and tau-rich AD brain homogenates was determined by saturation and competition binding assays. The binding selectivity of compounds to tau pathology was evaluated by autoradiography of AD brain sections. The pharmacokinetics of compounds were assessed in biodistribution studies in normal mice. A 14-d toxicity study with intravenous administration of compounds was performed using rats and mice. **Results:** In vitro binding assays demonstrated higher binding affinity of THK-5105 and THK-5117 than THK-523 to tau protein aggregates and tau-rich AD brain homogenates. Autoradiographic analyses of AD brain sections showed that these radiotracers preferentially bound to neurofibrillary tangles and neuropil threads, which colocalized with Gallyas-positive and immunoreactive tau protein deposits. The distribution of this radiotracer binding in AD brain sections was completely different from that of ^{11}C-Pittsburgh compound B, showing preferential binding to amyloid plaques. Furthermore, these derivatives demonstrated abundant initial brain uptake and faster clearance in normal mice than ^{18}F-THK-523 and other reported ^{18}F-labeled radiotracers. THK-5105 and THK-5117 showed no toxic effects related to the administration of these compounds in mice and rats and no significant binding for various neuroreceptors, ion channels, and transporters at 1-μM concentrations. **Conclusion:** ^{18}F-labeled THK-5105 and THK-5117 are promising candidates as PET tau imaging radiotracers.

Received Nov. 19, 2012; revision accepted Feb. 19, 2013.
For correspondence or reprints contact: Nobuyuki Okamura, 2-1, Seiryo-machi, Aoba-ku, Sendai 980-8575 Japan.
E-mail: nookamura@med.tohoku.ac.jp
Published online Jul. 15, 2013.

Key Words: Alzheimer disease; tau; neurofibrillary tangles; positron emission tomography; molecular imaging

J Nucl Med 2013; 54:1420–1427
DOI: 10.2967/jnumed.112.117341

Alzheimer disease (AD) is the most common cause of dementia in the elderly. At present, approximately 18 million people worldwide have AD, and this number is estimated to double by 2025 (*1*). The major pathologic hallmarks of AD are senile plaques (SPs) and neurofibrillary tangles (NFTs). SPs are composed of amyloid-β protein (Aβ), a 39–43 amino acid protein product derived from the proteolytic cleavage of the amyloid precursor protein. Abnormalities in the production or clearance of Aβ are considered to be the initiating events in AD pathogenesis (*2*). Excessive Aβ concentrations lead to its aggregation and formation of SPs, followed by NFT formations, synaptic dysfunction, and neuronal death. NFTs are composed of hyperphosphorylated tau, a microtubule-associated protein that stabilizes microtubule assembly in axons (*3*). Tau accumulation is also recognized as neuropil threads and dystrophic neurites in the AD brain (*4*). Phosphorylation of tau decreases its ability to bind to microtubules, which are destabilized, leading to neuronal death. NFT lesions follow a stereotypical pattern, initially appearing in the transentorhinal cortex, followed by the entorhinal cortex and the hippocampus, and subsequently the neocortex (*5*). In AD patients, the severity of tau pathology is closely related to neuronal loss (*6,7*) and cognitive impairment (*8,9*). The deposition of NFTs is thought to begin before extensive neuronal loss and cognitive decline occur. Thus, noninvasive detection of tau pathology would be useful to predict future cognitive decline in the preclinical stages of AD and to track disease progression before extensive neuronal loss occurs.

Several researchers have focused on developing radiotracers for imaging tau pathology in the human brain (*10–17*). Tau imaging radiotracers need to cross the blood–brain barrier and to have a high binding affinity to NFTs with minimal nonspecific binding (*18*). 2-(1-(6-[(2-^{18}F-fluoroethyl)(methyl)amino]-2-naphthyl)ethylidene)malononitrile (^{18}F-FDDNP) is claimed as the only PET tracer that allows measurement of the amount of tau protein

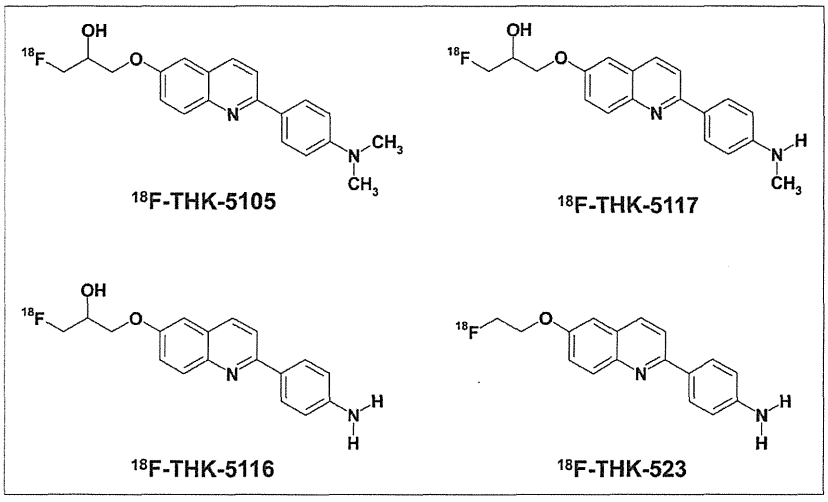

FIGURE 1. Chemical structures of ^{18}F-THK-5105, ^{18}F-THK-5116, ^{18}F-THK-5117, and ^{18}F-THK-523.

deposits in the human brain (*19*). However, ^{18}F-FDDNP was found to have lower binding affinity for protein fibrils than ^{11}C-Pittsburgh compound B (^{11}C-PiB) (*20,21*). In addition, this tracer has been claimed to bind to both SPs and NFTs equally (*22*). In the neocortex of the AD brain, SPs and NFTs colocalize with each other, where Aβ concentrations are 5–20 times higher than that of tau (*23,24*). In such cases, the signal from the SPs would be so overwhelming that it would obscure the signal from the NFTs. Therefore, the development of selective tau imaging tracers is necessary for accurate and quantitative evaluation of tau pathology in AD.

In the past few years, we also have screened more than 2,000 compounds to develop novel radiotracers with high affinity and selectivity for tau aggregates. Consequently, we identified a series of novel quinoline and benzimidazole derivatives that bind NFTs and, to a lesser extent, Aβ plaques (*10*). Serial analyses of these compounds led to the design and synthesis of the novel tau imaging agent ^{18}F-6-(2-fluoroethoxy)-2-(4-aminophenyl)quinoline (^{18}F-THK-523) (*15,17*). Preclinical analyses of ^{18}F-THK-523 indicated that this tracer selectively labels tau pathology in the AD brain. However, the preclinical data suggest that the pharmacokinetics and binding characteristics of ^{18}F-THK-523 might not reach the necessary optimal levels required for PET tracers. Through our optimization process, we developed novel ^{18}F-labeled 2-arylquinoline derivatives that are promising candidates for in vivo tau imaging probes. In this study, we performed the preclinical evaluation of the binding and pharmacokinetic properties of these compounds.

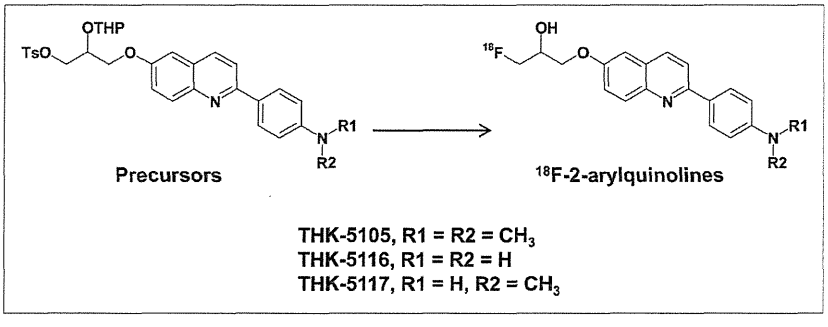

FIGURE 2. Radiosynthesis scheme of ^{18}F-2-arylquinolines.

MATERIALS AND METHODS

Synthesis and Radiosynthesis of 2-Arylquinoline Derivatives

The chemical structures of 6-[(3-^{18}F-fluoro-2-hydroxy)propoxy]-2-(4-dimethylaminophenyl)quinoline (^{18}F-THK-5105), 6-[(3-^{18}F-fluoro-2-hydroxy)propoxy]-2-(4-methylaminophenyl)quinoline (^{18}F-THK-5117), 6-[(3-^{18}F-fluoro-2-hydroxy)propoxy]-2-(4-aminophenyl)quinoline (^{18}F-THK-5116), and ^{18}F-THK-523 are shown in Figure 1. ^{18}F-THK-5105, ^{18}F-THK-5116, and ^{18}F-THK-5117 were prepared from the corresponding tosylate precursors according to the scheme as indicated in the Figure 2. Details on their syntheses will be described elsewhere (S. Furumoto et al., unpublished data, 2013). Briefly, the aqueous $^{18}F^-$ contained in the K_2CO_3 solution (1.59–3.69 GBq) and Kryptofix222 (15 mg) were placed in a brown vial. Water was removed by azeotropic evaporation with acetonitrile. After being dried, the activated ^{18}F-KF/Kryptofix222 was reacted with the precursor (3 mg) in dimethylsulfoxide (0.7 mL) at 110°C for 10 min. Then, 2 M HCl was added to the solution, followed by an additional 3-min reaction for deprotection of the hydroxyl group. After neutralization with 4 M AcOK, the product was purified by semipreparative high-performance liquid chromatography (HPLC) (column: Inertsil ODS-4 [GL Sciences, Inc.]; mobile phase: 20 mM NaH_2PO_4/acetonitrile [55/45 for THK-5105 and THK-5117, 65/35 for THK-5116]; flow rate: 5.0 mL/min). The radiolabeled product was dissolved in ethanol, dimethylsulfoxide, or saline with polysobate-80 (<0.1%) for biologic evaluation.

^{18}F-THK-523 and ^{18}F-FDDNP were also prepared in a manner similar to the one described above using the corresponding tosylate precursors reported previously (*15,25,26*). ^{11}C-PiB was radiolabeled using its precursor (2-(4-aminophenyl)-6-methoxymethoxybenzothiazole) and ^{11}C-methyl triflate, as previously described (*27*).

Determination of Log P Values

Log P values were determined by the HPLC method according to the guideline of the Organisation for Economic Co-operation and Development (OECD Guideline for Testing of Chemicals: Partition Coefficient (n-octanol/water), High Performance Liquid Chromatography [HPLC] Method), with slight modification. Briefly, 12 reference compounds whose log P values ranged between 0.5 and 4.0 were analyzed by HPLC under the following conditions: HPLC, a JASCO LC-2000 Plus series (JASCO); column, Inertsil ODS-4 (4.6 × 150 mm, 5 μm; GL Sciences, Inc.); mobile phase, 20 mM NaH_2PO_4 (pH 7.4)/acetonitrile (55/45); flow rate, 1.5 mL/min; ultraviolet absorbance, 245 nm; and column temperature, 40°C. Then, a calibration curve of log (tR − t0) (tR, retention time; t0, dead time) versus log P of each reference compound was created (R^2 = 0.9469). Test compounds listed in Table 1 were also analyzed by the same HPLC method to measure log (tR − t0) values that were used for determination of log P values from the calibration curve.

In Vitro Binding Assays

Synthetic human Aβ1–42 was purchased from Peptide Institute Inc. Recombinant K18ΔK280-tau protein was obtained from Life Technologies Japan Ltd. Fibrils of